

## Data Based Reconstruction of Duplex Networks\*

Chuang Ma<sup>†</sup>, Han-Shuang Chen<sup>‡</sup>, Xiang Li<sup>§</sup>, Ying-Cheng Lai<sup>¶</sup>, and Hai-Feng Zhang<sup>||</sup>

**Abstract.** It has been recognized that many complex dynamical systems in the real world require a description in terms of multiplex networks, where a set of common, mutually connected nodes belong to distinct network layers and play a different role in each layer. In spite of recent progress toward data based inference of single-layer networks, to reconstruct complex systems with a multiplex structure remains largely open. In this paper, we articulate a mean-field based maximum likelihood estimation framework to address this problem. In a concrete manner, we reconstruct a class of prototypical duplex network systems hosting two categories of spreading dynamics, and we show that the structures of both layers can be simultaneously reconstructed from time series data. In addition to validating the framework using empirical and synthetic duplex networks, we carry out a detailed analysis to elucidate the impacts of network and dynamics parameters on the reconstruction accuracy and the robustness.

**Key words.** multiplex networks, network reconstruction, mean-field approximation, maximum likelihood estimation

**AMS subject classifications.** 37N99, 62P25

**DOI.** 10.1137/19M1254040

**1. Introduction.** In mathematical and physical sciences, it is recognized that the “inverse problem” is often significantly more difficult than the “forward problem.” In particular, given a system with a known structure and a set of mathematical equations, the forward problem focuses on analyzing and possibly solving the equations (analytically or numerically) to uncover and understand the behaviors of the system. For the inverse problem, the system structure and equations are unknown but only observational or measured data are available. The task is to infer the intrinsic structure and dynamics of the system from the data. In network science and engineering, to reconstruct the topology of an unknown complex network

---

\*Received by the editors April 3, 2019; accepted for publication (in revised form) by I. Belykh October 25, 2019; published electronically January 7, 2020.

<https://doi.org/10.1137/19M1254040>

**Funding:** This work was supported by NSFC under grant 61973001, 11875069, and 61473001. The work of the third author was supported by the National Science Fund for Distinguished Young Scholars of China (61425019) and NSFC under grant 71731004. The work of the fourth author was supported by ONR through grant N00014-16-1-2828.

<sup>†</sup>School of Internet, Anhui University, Hefei 230601, China ([chuang\\_m@126.com](mailto:chuang_m@126.com)).

<sup>‡</sup>School of Physics and Material Science, Anhui University, Hefei 230601, China ([chenhshf@ahu.edu.cn](mailto:chenhshf@ahu.edu.cn)).

<sup>§</sup>Adaptive Networks and Control Laboratory, Department of Electronic Engineering, and Center of Smart Networks and Systems, School of Information Science and Engineering, Fudan University, Shanghai 200433, China ([lix@fudan.edu.cn](mailto:lix@fudan.edu.cn)).

<sup>¶</sup>School of Electrical, Computer, and Energy Engineering, Arizona State University, Tempe, AZ 85287 ([Ying-Cheng.Lai@asu.edu](mailto:Ying-Cheng.Lai@asu.edu)).

<sup>||</sup>Corresponding author. School of Mathematical Science, Anhui University, Hefei 230601, China ([haifengzhang1978@gmail.com](mailto:haifengzhang1978@gmail.com)).

and to map out the dynamical process on the network based solely on measured time series or data have been active areas of interdisciplinary research [15, 17, 34, 4, 13, 49, 3, 42, 31, 12, 33, 35, 23, 20, 36, 45, 2, 38, 40, 19, 52, 8, 43, 39, 37, 9, 44, 6, 25, 7, 30, 50]. A variety of approaches have been devised, which include those based on collective dynamics [49, 52, 42, 43, 32, 26], stochastic analysis [27, 25], optimal causation entropy [41], compressive sensing [46, 37, 39, 30], etc. However, previous works focused on single-layer networks. The goal of this paper is to address the significantly more challenging problem of data based reconstruction of *multiplex* networks.

A complex system in the real world, such as modern infrastructure or a social or transportation system, consists of many units connected by different types of relationship. For example, a social network contains different types of ties among people and a transportation system comprises multiple types of travel platforms. Such systems require a description in terms of multiplex networks [5, 16, 11, 22, 10, 21]. Previous efforts in multiplex networks focused on the forward problem to unearth the mathematical properties and the associated physical phenomena [48]. *The main difficulty that one has to overcome to address the inverse problem of multiplex networked systems lies in the distinct, possibly quite diverse yet interwoven collective dynamics in different layers.* For example, the outbreak of an epidemic in human society induces diffusion of awareness in online social networks, leading to two types of mutually coupled spreading dynamics [18], each in a different network layer. Another example is that opinions can diffuse through different channels (layers) and interact with each other.

In this paper, we develop a reconstruction framework based on mean-field maximum likelihood estimation (MLE) to address the problem of data based reconstruction of multiplex networks. As the first attempt, we focus on duplex networked systems—perhaps the most extensively studied multiplex networks that are relevant to real world situations such as complex cyberphysical systems. We assume that each layer hosts a distinct type of spreading dynamics and the two types of processes are interwoven. In particular, one (physical) layer hosts the susceptible-infected-susceptible (SIS) type of spreading dynamics, while the other (virtual) layer is a social network with information spreading governed by the unaware-aware-unaware (UAU) process [18]. Provided that binary time series data are available from both layers, we show that our framework is capable of accurately reconstructing the full topology of each layer for a large number of empirical and synthetic networks. We elucidate the impacts of network structural and dynamics parameters on reconstruction accuracy, such as the average degree, interlayer coupling, and heterogeneity in the spreading rates. The effect of noise is also investigated. Our framework represents an effort to assess the “internal gear” of complex systems with a duplex structure.

**2. UAU-SIS dynamics on duplex networks.** The UAU-SIS model was originally articulated to study the competition between social awareness and disease spreading on double-layer networks, where the physical contact layer supports an epidemic process and the virtual contact (the case of UAU-SIR dynamics on duplex networks is studied—see Appendix E, where  $R$  is the recovered state and the recovered nodes cannot be infected again). The two layers share exactly the same set of nodes but their connection patterns are different.

Spreading of awareness in the virtual layer is described by the UAU spreading model, in which an unaware (U) node may enter an aware (A) state by two ways: (1) it is informed by one A-state neighbor in the virtual layer with probability  $\lambda$ , or (2) the node is infected by the epidemic in the contact layer, so it automatically enters an A-state. Meanwhile, an A-state node can lose awareness and returns to the U-state with probability  $\delta$ .

Epidemic dynamics in the physical layer are of the SIS type, where an infected (I) node can infect its susceptible (S) neighbors with probability  $\beta$ , and an I-state node returns to the S-state with probability  $\mu$ . Upon considering the effect of awareness in the virtual layers, the probabilities of being infected are different, depending on whether the S-state node is in the A-state or the U-state. We set  $\beta_A$  and  $\beta_U$ , respectively, and it is reasonable to assume that  $\beta_U \geq \beta_A$ . Figure 1 presents a schematic illustration of the duplex network with the described interacting dynamical processes.

According to the description of the UAU-SIS spreading model on the duplex network, one knows that each node has three possible states: unaware and susceptible (US) state, aware (US)

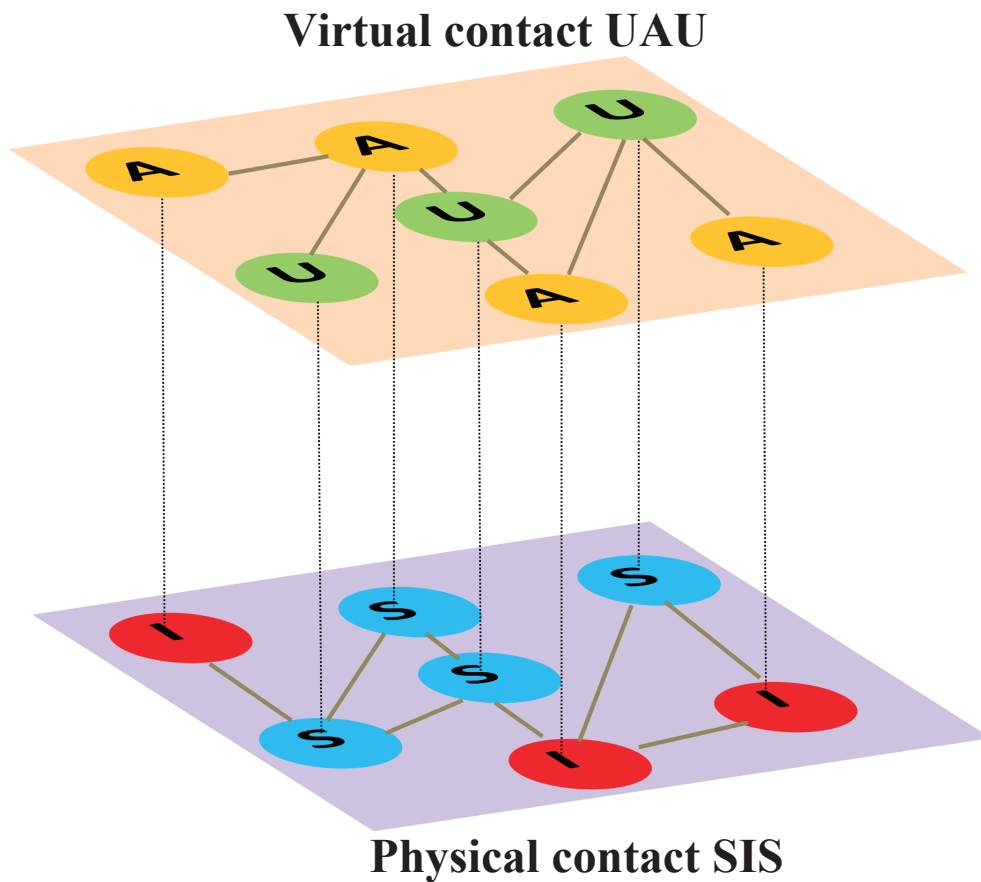


**Figure 1.** Schematic illustration of a duplex network hosting two kinds of spreading dynamics. The upper layer (virtual contact) supports awareness diffusion, where each node has two possible states: unaware (U) or aware (A). The bottom layer (physical contact) takes place epidemic spreading dynamics, where a node can be in the susceptible (S) or infected (I) state.

and susceptible (AS) state, and aware and infected (AI) state. The unaware and infected (UI) state cannot appear since an infected node *immediately enters* an A-state.

Let  $\bar{s}_t^i$  and  $s_t^i$  denote the state of node  $i$  at time  $t$  in the virtual layer and the physical layer, respectively.  $\bar{s}_t^i = 0$  (or 1) indicates that node  $i$  is in a U-state (A-state), and  $s_t^i = 0$  (or 1) indicates that node  $i$  is in an S-state (I-state). Moreover, the connections of node  $i$  in the virtual and physical layers are specified by the vectors  $\mathbf{a}^i$  and  $\mathbf{b}^i$ , respectively, where  $a_j^i = 1$  indicates that node  $j$  is a neighbor of node  $i$  in the virtual layer and  $a_j^i = 0$  otherwise, and  $b_j^i$  is defined similarly. Therefore,  $\sum_{j \neq i} a_j^i \bar{s}_t^j$  (or  $\sum_{j \neq i} b_j^i s_t^j$ ) depicts the number of A-neighbors (I-neighbors) of node  $i$ .

Three probabilities are needed to describe the network spreading dynamics: (1)  $r_t^i$ , the probability that node  $i$  is not informed by any neighbor, (2)  $q_{U,t}^i$ , the probability that U-state node  $i$  is not infected by any neighbor, and (3)  $q_{A,t}^i$ , the probability that A-state node  $i$  is not infected by any neighbor. In the absence of any dynamical correlation, the three probabilities are given as

$$(2.1) \quad \begin{aligned} r_t^i &= (1 - \lambda^i)^{\sum_{j \neq i} a_j^i \bar{s}_t^j}, \\ q_{U,t}^i &= (1 - \beta_U^i)^{\sum_{j \neq i} b_j^i s_t^j}, \\ q_{A,t}^i &= (1 - \beta_A^i)^{\sum_{j \neq i} b_j^i s_t^j}. \end{aligned}$$

A tacit assumption in [18] is that diffusion of awareness in the virtual layer occurs before epidemic spreading in the physical layer. In our work, we do not require that the two types of spreading dynamics occur in any particular order. Figure 2 presents the transition probability tree of the UAU-SIS coupling dynamics on the duplex networks.

Figure 2 and (2.1) indicate that the transition probabilities of node  $i$  from the US state to the US, AS, and AI states are

$$(2.2) \quad \begin{aligned} P^{US \rightarrow US} &= r_t^i q_{U,t}^i, \\ P^{US \rightarrow AS} &= (1 - r_t^i) q_{U,t}^i, \\ P^{US \rightarrow AI} &= r_t^i (1 - q_{U,t}^i) + (1 - r_t^i) (1 - q_{U,t}^i) = 1 - q_{U,t}^i. \end{aligned}$$

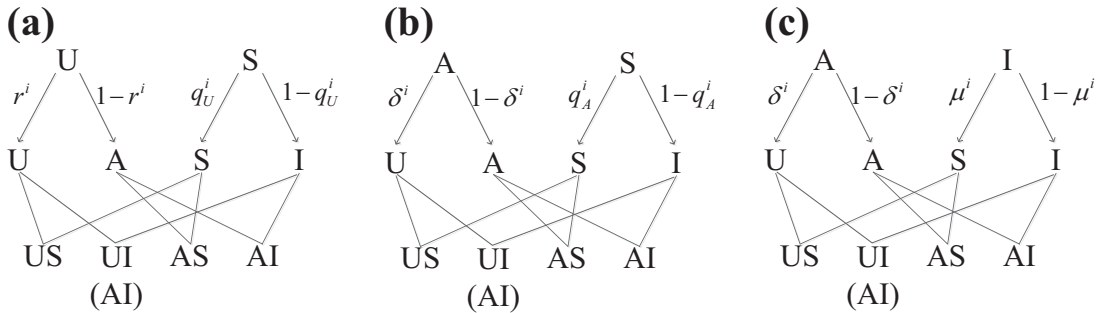


**Figure 2.** Transition probability tree of coupled UAU-SIS dynamics on duplex networks. AI, aware and infected; UI, unaware and infected (redundant to the AI state); AS, aware and susceptible; and US, unaware and susceptible.

The transition probabilities of node  $i$  from the AS state to the US, AS, and AI states are

$$(2.3) \quad \begin{aligned} P^{AS \rightarrow US} &= \delta^i q_{A,t}^i, \\ P^{AS \rightarrow AS} &= (1 - \delta^i) q_{A,t}^i, \\ P^{AS \rightarrow AI} &= \delta^i (1 - q_{A,t}^i) + (1 - \delta^i) (1 - q_{A,t}^i) = 1 - q_{A,t}^i. \end{aligned}$$

Also, the transition probabilities of node  $i$  from the AI state to the US, AS, and AI states are

$$(2.4) \quad \begin{aligned} P^{AI \rightarrow US} &= \delta^i \mu^i, \\ P^{AI \rightarrow AS} &= (1 - \delta^i) \mu^i, \\ P^{AI \rightarrow AI} &= 1 - \mu^i. \end{aligned}$$

**3. Theoretical framework of reconstruction.** Say only the states  $\bar{s}_{t_m}^i$  and  $s_{t_m}^i$  ( $i = 1, \dots, N$ ) at time  $t_m$  (not necessarily uniform) are recorded, where  $N$  is the network size. Our reconstruction framework consists of three steps: (1) to establish the likelihood function of the coupled dynamics, (2) to apply the mean-field approximation to enable MLE, and (3) to transform the MLE problem into two solvable linear systems—one for each layer with solutions representing the neighbors of each node in the layer.

**3.1. Establish the likelihood function.** For node  $i$ , if we know all nodes' states in two layers (i.e.,  $\bar{s}_{t_m}^j$  and  $s_{t_m}^j$ ,  $j = 1, 2, \dots, N$ ), its connections in the virtual and physical layers (i.e.,  $\mathbf{a}^i$  and  $\mathbf{b}^i$ ), and the parameters in the dynamics (i.e.,  $\lambda^i$ ,  $\beta_U^i$ ,  $\beta_A^i$ ,  $\delta^i$ , and  $\mu^i$ ), then the joint probability (likelihood function) of node  $i$  at all the next time states is

$$(3.1) \quad P \left( \{ \bar{s}_{t_m+1}^i, s_{t_m+1}^i \}_{m=1 \dots M} \mid \{ \bar{s}_{t_m}^j, s_{t_m}^j \}_{j=1 \dots N, m=1 \dots M}, \mathbf{a}^i, \mathbf{b}^i, \lambda^i, \beta_U^i, \beta_A^i, \delta^i, \mu^i \right) \\ = \prod_m \left\{ \begin{aligned} & \left[ \begin{aligned} & \left( r_{t_m}^i q_{U,t_m}^i \right)^{(1-\bar{s}_{t_m+1}^i)(1-s_{t_m+1}^i)} \left( 1 - q_{U,t_m}^i \right)^{\bar{s}_{t_m+1}^i s_{t_m+1}^i} \end{aligned} \right]^{(1-\bar{s}_{t_m}^i)(1-s_{t_m}^i)} \\ & \times \left[ \begin{aligned} & \left( (1 - r_{t_m}^i) q_{U,t_m}^i \right)^{\bar{s}_{t_m+1}^i (1-s_{t_m+1}^i)} \end{aligned} \right] \end{aligned} \right\} \\ \times \left\{ \begin{aligned} & \left[ \begin{aligned} & \left( \delta^i q_{A,t_m}^i \right)^{(1-\bar{s}_{t_m+1}^i)(1-s_{t_m+1}^i)} \left( (1 - \delta^i) q_{A,t_m}^i \right)^{\bar{s}_{t_m+1}^i (1-s_{t_m+1}^i)} \end{aligned} \right]^{\bar{s}_{t_m}^i (1-s_{t_m}^i)} \\ & \times \left[ \begin{aligned} & \left( 1 - q_{A,t_m}^i \right)^{\bar{s}_{t_m+1}^i s_{t_m+1}^i} \end{aligned} \right] \end{aligned} \right\} \\ \times \left\{ \begin{aligned} & \left[ \begin{aligned} & \left( \delta^i \mu^i \right)^{(1-\bar{s}_{t_m+1}^i)(1-s_{t_m+1}^i)} \left( (1 - \delta^i) \mu^i \right)^{\bar{s}_{t_m+1}^i (1-s_{t_m+1}^i)} \end{aligned} \right]^{\bar{s}_{t_m}^i s_{t_m}^i} \\ & \times \left[ \begin{aligned} & \left( 1 - \mu^i \right)^{\bar{s}_{t_m+1}^i s_{t_m+1}^i} \end{aligned} \right] \end{aligned} \right\} \end{aligned} \right\}.$$

As we know, one node will enter the A-state immediately if it is infected (i.e.,  $s_{t_m}^i = 1$  indicates  $\bar{s}_{t_m}^i = 1$ ). As a result, we have  $\bar{s}_{t_m+1}^i s_{t_m+1}^i = s_{t_m+1}^i$  and  $\bar{s}_{t_m}^i s_{t_m}^i = s_{t_m}^i$ . Also, a node in the U-state cannot be in the I-state, (i.e.,  $\bar{s}_{t_m}^i = 0$  indicates  $s_{t_m}^i = 0$ ), which leads to  $(1 - \bar{s}_{t_m}^i)(1 - s_{t_m}^i) = 1 - \bar{s}_{t_m}^i$  and  $(1 - \bar{s}_{t_m+1}^i)(1 - s_{t_m+1}^i) = 1 - \bar{s}_{t_m+1}^i$ .

Even though (3.1) seems to be complicated, it can be reduced to some simple forms when some explicit conditions are given. For example, assuming that node  $i$  at  $t_m$  is in the US state (i.e.,  $\bar{s}_{t_m}^i = 0$  and  $s_{t_m}^i = 0$ ), then only one term is retained in the product, namely,

$$\left[ \left( r_{t_m}^i q_{U,t_m}^i \right)^{(1-\bar{s}_{t_m+1}^i)(1-s_{t_m+1}^i)} \left( (1-r_{t_m}^i) q_{U,t_m}^i \right)^{\bar{s}_{t_m+1}^i(1-s_{t_m+1}^i)} \left( 1-q_{U,t_m}^i \right)^{\bar{s}_{t_m+1}^i s_{t_m+1}^i} \right],$$

which can be further reduced to  $(1-r_{t_m}^i)q_{U,t_m}^i$  if  $\bar{s}_{t_m+1}^i = 1$  and  $s_{t_m+1}^i = 0$  (i.e., in the AS state at the next time step  $t_m + 1$ ). In sum, (3.1) contains all the transition probabilities in (2.2)–(2.4).

After implementing some algebraic operations on the logarithmic form of (3.1), one has the following equation:

$$(3.2) \quad L(\mathbf{a}^i, \mathbf{b}^i, \lambda^i, \beta_U^i, \beta_A^i, \delta^i, \mu^i) = L_0(\delta^i, \mu^i) + L_1(\mathbf{a}^i, \lambda^i) + L_2(\mathbf{b}^i, \beta_U^i, \beta_A^i),$$

where

$$(3.3) \quad L_0(\delta^i, \mu^i) = \sum_m \left[ \bar{s}_{t_m}^i (1 - \bar{s}_{t_m+1}^i) \ln(\delta^i) + \bar{s}_{t_m}^i \bar{s}_{t_m+1}^i (1 - s_{t_m+1}^i) \ln(1 - \delta^i) \right. \\ \left. + s_{t_m}^i (1 - s_{t_m+1}^i) \ln(\mu^i) + s_{t_m}^i s_{t_m+1}^i \ln(1 - \mu^i) \right].$$

The quantity that does contain the information is  $L_1(\mathbf{a}^i, \lambda^i)$ , which depends on the connectivity of node  $i$  in the virtual layer. It can be written as

$$(3.4) \quad L_1(\mathbf{a}^i, \lambda^i) = \sum_m \left[ \bar{X}_{t_m}^i \ln \left( (1 - \lambda^i)^{\sum_{j \neq i} a_j^i \bar{s}_{t_m}^j} \right) + \bar{Y}_{t_m}^i \ln \left( 1 - (1 - \lambda^i)^{\sum_{j \neq i} a_j^i \bar{s}_{t_m}^j} \right) \right]$$

with  $\bar{X}_{t_m}^i = (1 - \bar{s}_{t_m}^i)(1 - \bar{s}_{t_m+1}^i)$  and  $\bar{Y}_{t_m}^i = (1 - \bar{s}_{t_m}^i)(1 - s_{t_m+1}^i)\bar{s}_{t_m+1}^i$ .

Similarly, the quantity  $L_2(\mathbf{b}^i, \beta_U^i, \beta_A^i)$  that depends on the connectivity of node  $i$  in the physical layer is given by

$$(3.5) \quad L_2(\mathbf{b}^i, \beta_U^i, \beta_A^i) = \sum_m \left\{ \left[ X_{U,t_m}^i \ln \left( (1 - \beta_U^i)^{\sum_{j \neq i} b_j^i s_{t_m}^j} \right) + Y_{U,t_m}^i \ln \left( 1 - (1 - \beta_U^i)^{\sum_{j \neq i} b_j^i s_{t_m}^j} \right) \right] \right. \\ \left. + \left[ X_{A,t_m}^i \ln \left( (1 - \beta_A^i)^{\sum_{j \neq i} b_j^i s_{t_m}^j} \right) + Y_{A,t_m}^i \ln \left( 1 - (1 - \beta_A^i)^{\sum_{j \neq i} b_j^i s_{t_m}^j} \right) \right] \right\},$$

where  $X_{U,t_m}^i = (1 - \bar{s}_{t_m}^i)(1 - s_{t_m+1}^i)$ ,  $Y_{U,t_m}^i = (1 - \bar{s}_{t_m}^i)s_{t_m+1}^i$ ,  $X_{A,t_m}^i = \bar{s}_{t_m}^i(1 - s_{t_m}^i)(1 - s_{t_m+1}^i)$ , and  $Y_{A,t_m}^i = \bar{s}_{t_m}^i(1 - s_{t_m}^i)s_{t_m+1}^i$ .

Equation (3.2) indicates that the problem of the MLE can be realized by separately maximizing the likelihood function  $L_0$ ,  $L_1$ , and  $L_2$ . However, (3.3) does not rely on any information about the network structure. Therefore, we can separately maximize the likelihood function  $L_1$  and  $L_2$ , which can help us solve the connections of node  $i$  in the virtual layer (i.e.,  $\mathbf{a}^i$ ) and in the physical layer (i.e.,  $\mathbf{b}^i$ ). In principle, (3.2) indicates that one can maximize  $L_1$  and  $L_2$  with respect to  $a_j^i$  and  $b_j^i$ , respectively, to uncover the connectivity of node  $i$ . However, the conventional maximization process leads to equations that cannot be solved because the quantity  $a_j^i$  ( $b_j^i$ ) appears in the exponential term and the values of  $\lambda^i$  (or  $\beta_U^i$ ,  $\beta_A^i$ ) are unknown. In the following steps, we will demonstrate how to exploit the mean-field approximation to overcome the difficulties and transform the problem of maximizing  $L_1$  and  $L_2$  into two solvable linear systems of equations. In the main context, we mainly focus on how to reconstruct the virtual layer, the reconstruction process of the physical layer is similar, so it is summarized in Appendix A.

**3.2. Mean-field approximation.** The maximum value of  $L_1$  cannot be obtained straightforwardly by setting zero as its derivative with respect to  $a_j^i$ , because  $a_j^i$  appears in the exponential term and the values of  $\lambda^i$  are unknown. We resort to the mean-field approximation to solve this problem. Specifically, for node  $i$  in the virtual layer, the fraction  $\sum_{j \neq i} \bar{s}_{t_m}^j a_j^i$  of A-neighbors is approximately equal to the fraction of A-nodes in the whole layer excluding node  $i$  itself:

$$(3.6) \quad \sum_{j \neq i} \bar{s}_{t_m}^j a_j^i \approx \frac{\bar{k}^i}{N-1} \bar{\theta}_{t_m}^i,$$

where  $\bar{k}^i$  is the degree of node  $i$  in the virtual layer, and  $\bar{\theta}_{t_m}^i = \sum_{j \neq i} \bar{s}_{t_m}^j$  is the number of A-nodes excluding node  $i$  itself. A new unknown parameter  $\bar{k}^i$  emerges in (3.4) when we substitute (3.6) into (3.4). To simplify the analysis, we let  $\bar{\gamma}^i = (1 - \lambda^i)^{\frac{\bar{k}^i}{N-1}}$ , leading to  $(1 - \lambda^i)^{\sum_{j \neq i} a_j^i \bar{s}_{t_m}^j} = (1 - \lambda^i)^{\frac{\bar{k}^i}{N-1} \bar{\theta}_{t_m}^i} = (\bar{\gamma}^i)^{\bar{\theta}_{t_m}^i}$ . Equation (3.4) can then be written concisely as

$$(3.7) \quad \hat{L}_1(\bar{\gamma}^i) = \sum_m \left[ \bar{X}_{t_m}^i \ln \left( (\bar{\gamma}^i)^{\bar{\theta}_{t_m}^i} \right) + \bar{Y}_{t_m}^i \ln \left( 1 - (\bar{\gamma}^i)^{\bar{\theta}_{t_m}^i} \right) \right].$$

Differentiating  $\hat{L}_1(\bar{\gamma}^i)$  with respect to  $\bar{\gamma}^i$  and setting it to zero, we get

$$(3.8) \quad \sum_m \bar{Y}_{t_m}^i \bar{\theta}_{t_m}^i \frac{(\bar{\gamma}^i)^{\bar{\theta}_{t_m}^i}}{1 - (\bar{\gamma}^i)^{\bar{\theta}_{t_m}^i}} = \sum_m \bar{X}_{t_m}^i \bar{\theta}_{t_m}^i.$$

From (3.8), one can numerically obtain the solution of  $\bar{\gamma}^i$  (denoted as  $\tilde{\gamma}^i$ ).

### 3.3. Transform the problem of MLE into two solvable linear systems of equations.

Treating  $a_l^i (l = 1, \dots, i-1, i+1, \dots, N)$  as a continuous variance, we can further differentiate (3.4) with respect to  $a_l^i$  and set it to zero, giving rise to

$$(3.9) \quad \sum_m \bar{Y}_{t_m}^i \bar{s}_{t_m}^l \frac{(1 - \lambda^i)^{\sum_{j \neq i} a_j^i \bar{s}_{t_m}^j}}{1 - (1 - \lambda^i)^{\sum_{j \neq i} a_j^i \bar{s}_{t_m}^j}} = \sum_m \bar{X}_{t_m}^i \bar{s}_{t_m}^l.$$

Obtaining analytical solutions of (3.9) is not feasible due to its nonlinear and high-dimensional nature (i.e.,  $(N-1) \times (N-1)$ ). We thus resort to the first-order Taylor expansion. In particular, we expand  $a^x / (1 - a^x)$  in the limit  $x \rightarrow x_0$  to obtain

$$(3.10) \quad \frac{a^x}{1 - a^x} \approx \frac{a^{x_0}}{1 - a^{x_0}} + \frac{a^{x_0} \ln a}{(1 - a^{x_0})^2} (x - x_0) = \frac{a^{x_0}}{1 - a^{x_0}} - \frac{a^{x_0} \ln a^{x_0}}{(1 - a^{x_0})^2} + \frac{a^{x_0} \ln a}{(1 - a^{x_0})^2} x.$$

Set  $x = \sum_{j \neq i} a_j^i \bar{s}_{t_m}^j$ ,  $a = 1 - \lambda^i$ , and  $x_0 = \frac{\bar{k}^i}{N-1} \bar{\theta}_{t_m}^i$  (here  $x \approx x_0$  according to (3.6)). Meanwhile, we have  $a^{x_0} = (\tilde{\gamma}^i)^{\bar{\theta}_{t_m}^i}$  since we have set  $\bar{\gamma}^i = (1 - \lambda^i)^{\frac{\bar{k}^i}{N-1}}$ . In this case,  $(1 - \lambda^i)^{\sum_{j \neq i} a_j^i \bar{s}_{t_m}^j} / 1 - (1 - \lambda^i)^{\sum_{j \neq i} a_j^i \bar{s}_{t_m}^j}$  in (3.9) can be expanded as in (3.10).

By letting

$$\bar{F}_{t_m}^i = \frac{(\tilde{\gamma}^i)^{\bar{\theta}_{t_m}^i}}{1 - (\tilde{\gamma}^i)^{\bar{\theta}_{t_m}^i}} - \frac{(\tilde{\gamma}^i)^{\bar{\theta}_{t_m}^i}}{\left(1 - (\tilde{\gamma}^i)^{\bar{\theta}_{t_m}^i}\right)^2} \bar{\theta}_{t_m}^i \ln \tilde{\gamma}^i \quad \text{and} \quad \bar{G}_{t_m}^i = \frac{(\tilde{\gamma}^i)^{\bar{\theta}_{t_m}^i}}{\left(1 - (\tilde{\gamma}^i)^{\bar{\theta}_{t_m}^i}\right)^2}$$

(note that these values can be calculated when the time series data are known), we transform (3.9) into a solvable linear system as

$$(3.11) \quad \sum_m \bar{Y}_{t_m}^i \bar{G}_{t_m}^i \bar{s}_{t_m}^l \ln(1 - \lambda^i) \sum_{j \neq i} a_j^i \bar{s}_{t_m}^j = \sum_m (\bar{X}_{t_m}^i - \bar{Y}_{t_m}^i \bar{F}_{t_m}^i) \bar{s}_{t_m}^l.$$

Further letting  $\bar{\Phi}_{t_m}^i = \bar{Y}_{t_m}^i \bar{G}_{t_m}^i$  and  $\bar{\Gamma}_{t_m}^i = \bar{X}_{t_m}^i - \bar{Y}_{t_m}^i \bar{F}_{t_m}^i$ , the linear system of equations (3.11) can be described in a matrix form:

$$(3.12) \quad \begin{bmatrix} \sum_m \bar{\Phi}_{t_m}^i \bar{\Gamma}_{1,1} & \cdots & \sum_m \bar{\Phi}_{t_m}^i \bar{\Gamma}_{1,i-1} & \sum_m \bar{\Phi}_{t_m}^i \bar{\Gamma}_{1,i+1} & \cdots & \sum_m \bar{\Phi}_{t_m}^i \bar{\Gamma}_{1,N} \\ \vdots & & \vdots & \vdots & & \vdots \\ \sum_m \bar{\Phi}_{t_m}^i \bar{\Gamma}_{i-1,1} & \cdots & \sum_m \bar{\Phi}_{t_m}^i \bar{\Gamma}_{i-1,i-1} & \sum_m \bar{\Phi}_{t_m}^i \bar{\Gamma}_{i-1,i+1} & \cdots & \sum_m \bar{\Phi}_{t_m}^i \bar{\Gamma}_{i-1,N} \\ \sum_m \bar{\Phi}_{t_m}^i \bar{\Gamma}_{i+1,1} & \cdots & \sum_m \bar{\Phi}_{t_m}^i \bar{\Gamma}_{i+1,i-1} & \sum_m \bar{\Phi}_{t_m}^i \bar{\Gamma}_{i+1,i+1} & \cdots & \sum_m \bar{\Phi}_{t_m}^i \bar{\Gamma}_{i+1,N} \\ \vdots & & \vdots & \vdots & & \vdots \\ \sum_m \bar{\Phi}_{t_m}^i \bar{\Gamma}_{N,1} & \cdots & \sum_m \bar{\Phi}_{t_m}^i \bar{\Gamma}_{N,i-1} & \sum_m \bar{\Phi}_{t_m}^i \bar{\Gamma}_{N,i+1} & \cdots & \sum_m \bar{\Phi}_{t_m}^i \bar{\Gamma}_{N,N} \end{bmatrix} \times \begin{bmatrix} a_1^i \ln(1 - \lambda^i) \\ \vdots \\ a_{i-1}^i \ln(1 - \lambda^i) \\ a_{i+1}^i \ln(1 - \lambda^i) \\ \vdots \\ a_N^i \ln(1 - \lambda^i) \end{bmatrix} = \begin{bmatrix} \sum_m \bar{\Gamma}_{t_m}^i \bar{s}_{t_m}^1 \\ \vdots \\ \sum_m \bar{\Gamma}_{t_m}^i \bar{s}_{t_m}^{i-1} \\ \sum_m \bar{\Gamma}_{t_m}^i \bar{s}_{t_m}^{i+1} \\ \vdots \\ \sum_m \bar{\Gamma}_{t_m}^i \bar{s}_{t_m}^N \end{bmatrix},$$

where  $\bar{\Gamma}_{l,k} = \bar{s}_{t_m}^l \bar{s}_{t_m}^k$ . The matrix on the left side (labeled as  $\mathbf{\Lambda}$ ) and the vector (labeled as  $\mathbf{\zeta}$ ) on the right side of (3.12) can be calculated from the time series of the nodal states. The vector

$$(3.13) \quad \boldsymbol{\eta} = [a_1^i \ln(1 - \lambda^i), \dots, a_{i-1}^i \ln(1 - \lambda^i), a_{i+1}^i \ln(1 - \lambda^i), \dots, a_N^i \ln(1 - \lambda^i)]^T$$

can then be solved, where  $T$  denotes transpose. Note that the quantity  $\ln(1 - \lambda^i) < 0$  is a constant even though  $\lambda^i$  is not given, implying that the value of  $-a_j^i \ln(1 - \lambda^i)$  is positively large for  $a_j^i = 1$  and near zero for  $a_j^i = 0$ .

Similarly, the connectivity of node  $i$  in the physical layer (i.e.,  $\mathbf{b}^i$ ) can be inferred by solving the following linear systems of equations (a detailed derivation process is summarized in Appendix A):

$$\begin{aligned}
(3.14) \quad & \begin{bmatrix} \sum_m \Phi_{t_m}^i I_{1,1} & \cdots & \sum_m \Phi_{t_m}^i I_{1,i-1} & \sum_m \Phi_{t_m}^i I_{1,i+1} & \cdots & \sum_m \Phi_{t_m}^i I_{1,N} \\ \vdots & & \vdots & \vdots & & \vdots \\ \sum_m \Phi_{t_m}^i I_{i-1,1} & \cdots & \sum_m \Phi_{t_m}^i I_{i-1,i-1} & \sum_m \Phi_{t_m}^i I_{i-1,i+1} & \cdots & \sum_m \Phi_{t_m}^i I_{i-1,N} \\ \sum_m \Phi_{t_m}^i I_{i+1,1} & \cdots & \sum_m \Phi_{t_m}^i I_{i+1,i-1} & \sum_m \Phi_{t_m}^i I_{i+1,i+1} & \cdots & \sum_m \Phi_{t_m}^i I_{i+1,N} \\ \vdots & & \vdots & \vdots & & \vdots \\ \sum_m \Phi_{t_m}^i I_{N,1} & \cdots & \sum_m \Phi_{t_m}^i I_{N,i-1} & \sum_m \Phi_{t_m}^i I_{N,i+1} & \cdots & \sum_m \Phi_{t_m}^i I_{N,N} \end{bmatrix} \\
& \times \begin{bmatrix} b_1^i \ln(1 - \beta_A^i) \\ \vdots \\ b_{i-1}^i \ln(1 - \beta_A^i) \\ b_{i+1}^i \ln(1 - \beta_A^i) \\ \vdots \\ b_N^i \ln(1 - \beta_A^i) \end{bmatrix} = \begin{bmatrix} \sum_m \Gamma_{t_m}^i s_{t_m}^1 \\ \vdots \\ \sum_m \Gamma_{t_m}^i s_{t_m}^{i-1} \\ \sum_m \Gamma_{t_m}^i s_{t_m}^{i+1} \\ \vdots \\ \sum_m \Gamma_{t_m}^i s_{t_m}^N \end{bmatrix},
\end{aligned}$$

where  $I_{l,k} = s_{t_m}^l s_{t_m}^k$ . From (3.14), the vector

$$(3.15) \quad \boldsymbol{\xi} = [b_1^i \ln(1 - \beta_A^i), \dots, b_{i-1}^i \ln(1 - \beta_A^i), b_{i+1}^i \ln(1 - \beta_A^i), \dots, b_N^i \ln(1 - \beta_A^i)]^T$$

can then be solved. Also,  $\ln(1 - \beta_A^i)$  is a constant even though the value of  $\beta_A^i$  is unknown. Thus, the neighbors of node  $i$  in the physical layer can be inferred from the vector  $\boldsymbol{\xi}$ . As a result, a threshold value can then be readily set to distinguish the existent from the nonexistent links: a pair of nodes  $i$  and  $l$  are connected in the virtual (or physical) layer if the value of  $-a_l^i \ln(1 - \lambda^i)$  ( $-b_l^i \ln(1 - \beta_A^i)$ ) is larger than the threshold (the criterion to choose the threshold is introduced in Appendix B).

#### 4. Main results.

**4.1. Reconstructing empirical duplex networks.** We first validate our framework using an empirical network of 61 employees in the Department of Computer Science at the University of Aarhus, the so-called CS-AARHUS network [29]. The original network has five layers. We regard the Facebook layer as the virtual layer and the other four offline layers (Leisure, Work, Co-authorship, Lunch) as the physical layer, as illustrated in Figures 3(a) and (b), respectively. Figures 3(c) and (d) show the values of characteristic quantities  $-a_l^i \ln(1 - \lambda^i)$  and  $-b_l^i \ln(1 - \beta_A^i)$  for the virtual and physical layers, where the blue and orange dots denote the existent and nonexistent links, respectively. We see that the values of the characteristic quantities are well separated by a distinct gap and can be unequivocally distinguished through a properly chosen threshold. For the physical layer in Figure 3(d), the gap between the blue and orange dots exhibits a decreasing trend with the nodal degree, indicating that the neighbors of larger degree nodes are harder to be detected because of neighborhood overlapping associated with such nodes. This result is consistent with previous findings [37, 27]. For the virtual layer (Figure 3(c)), the blue and orange dots for node 7 are overlapped even though

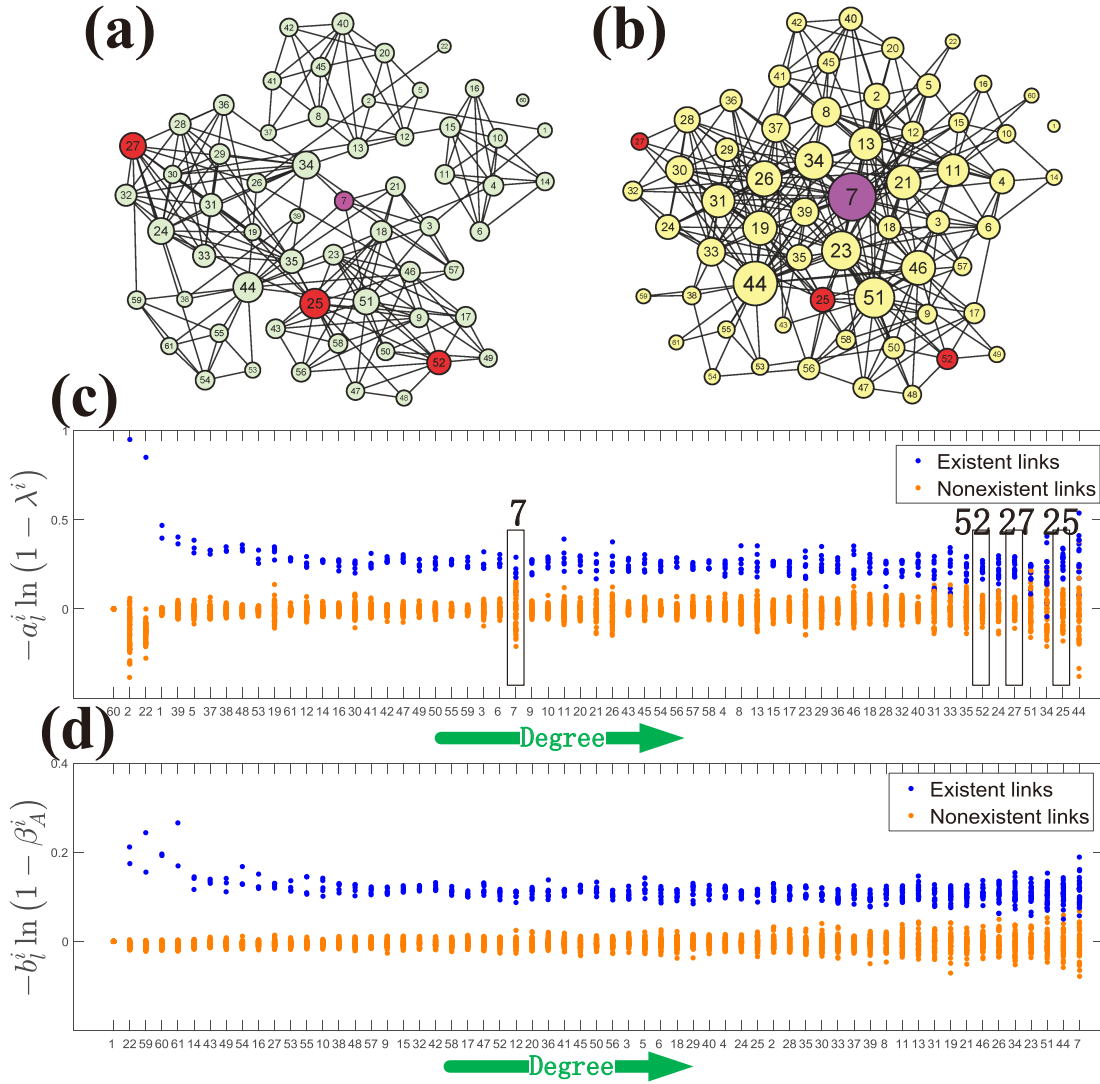


**Figure 3.** Reconstruction of the CS-AARHUS network. (a) Actual structure of the virtual contact layer (Facebook). (b) The structure of the physical layer. (c), (d) The values of  $-a_l^i \ln(1 - \lambda^i)$ ,  $i \neq l$ , and  $-b_l^i \ln(1 - \beta_A^i)$ ,  $i \neq l$ , respectively, versus the nodal degree. Each column gives the connectivity of a node, where the blue and orange dots denote the existent and nonexistent links, respectively. The length of the time series is  $M = 30000$ . The parameter values of the dynamical processes for all nodes are set as  $\lambda = 0.2$ ,  $\beta_U = 0.2$ ,  $\beta_A = 0.5\beta_U$ , and  $\mu = \delta = 0.8$ .

$\bar{k}^7 = 6$ , but there is a finite gap for large degree nodes, e.g., node 52 with  $\bar{k}^{52} = 10$ , node 27 with  $\bar{k}^{27} = 12$ , and node 25 with  $\bar{k}^{25} = 15$ . The relatively small gap of  $\bar{k}^7$  is due to the fact that the counterpart value in the physical layer is large:  $k^7 = 29$ , indicating that the node has been infected and is thus constantly in the A-state in the virtual layer (an infected node becomes aware immediately). As a result, the states of the neighbors of this node in the virtual layer have little influence on its state, making reconstruction difficult. For nodes with

large and small degrees in the virtual and physical layers, respectively, the transition from U to A is mainly determined by the states of the neighbors, facilitating reconstruction. In general, the structure of the physical layer has a significant effect on the reconstruction of the virtual layer, but the effect in the opposite direction is minimal. (In the main context, the parameter values of the dynamical processes for all nodes are the same. Figure 9 in Appendix C is given to validate the applicability of the reconstruction framework to spreading dynamics with heterogeneous rates.)

To better demonstrate the applicability of our reconstruction framework for complex duplex networks, we consider two duplex networks reconstructed from a temporal empirical network—a social evolution network [28]—as we were unable to reach empirical data directly from virtual/physical contact duplex networks. The social evolution network was conducted to study the daily life of more than 80% of the students residing in an MIT dormitory (the size of the network is  $N = 84$ ). The data recorded different social relationships among these students during 2008–2009. We choose the relationship networks in Facebook and CloseFriend as the virtual and physical layers, respectively. The first duplex network corresponds to the time period of October 2008, which is called MITSEN0810, with the average degrees of the virtual and physical layers being 27.71 and 7.26, respectively. The second duplex network is for the time period of April 2009, which is called MITSEN0904, with the average degrees of the virtual and physical layers being 31.98 and 8.19, respectively. The panels in the top and bottom rows of Figure 4 display the reconstruction accuracy in terms of the statistical quantities of AUROC (area under the receiver operating characteristic curve), AUPR (area under the precision recall curve), and Success rate (see Appendix D for the definitions of these evaluation metrics) versus the length of the time series for MITSEN0810 and MITSEN0904 networks, respectively. We have observed that the longer time series results in better reconstruction performance, and the reconstruction accuracy of the physical layer is higher than that of the virtual layer, consistent with the results in Figure 3.

**4.2. Performance analysis: Reconstructing synthetic duplex networks.** To understand the effect of interlayer coupling on reconstruction, we test a number of synthetic duplex networks: small-world (SW-SW) [47], Erdős–Rényi (ER-ER) [14], and Barabási–Albert (BA-BA) [1] duplex systems. For comparison, we include the special case where each layer is separately reconstructed without taking into account the other layer, which is equivalent to reconstructing a single-layer network (labeled as single). Figures 5(a)–(i) show that the reconstruction accuracy of the virtual layer is greatly reduced when a physical layer is introduced (e.g., blue  $\rightarrow$  black). Without the physical layer, the transition of an unaware node in the virtual layer to the aware state depends only on the states of its neighbors. With the presence of the physical layer, an A-node can spontaneously become aware once it is infected, “concealing” the information about the structure of the virtual layer. On the contrary, the reconstruction accuracy of the physical layer can be improved slightly (e.g., blue  $\rightarrow$  red) when the virtual layer is introduced, which reduces the ability to infect A-nodes and prevents too many nodes from being in the I-state, facilitating reconstruction. Figure 5 also illustrates that the reconstruction accuracy of the SW-SW duplex network is higher than that of the ER-ER duplex network and much higher than that of the

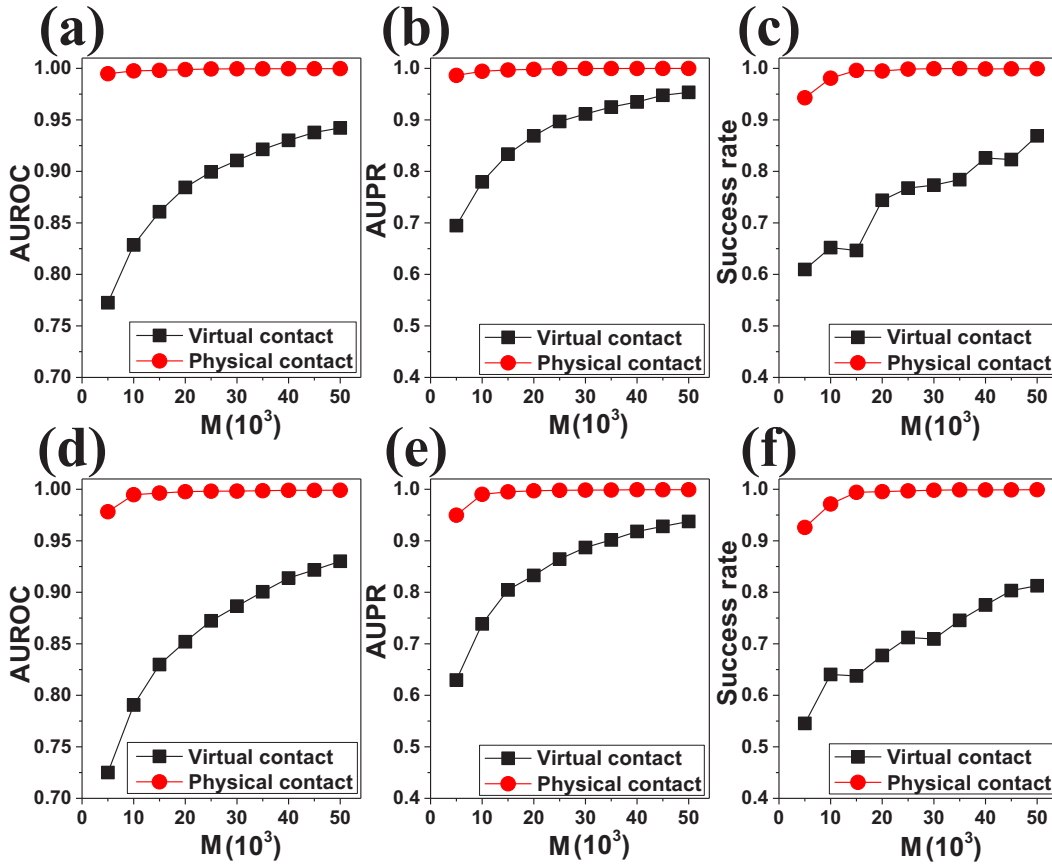
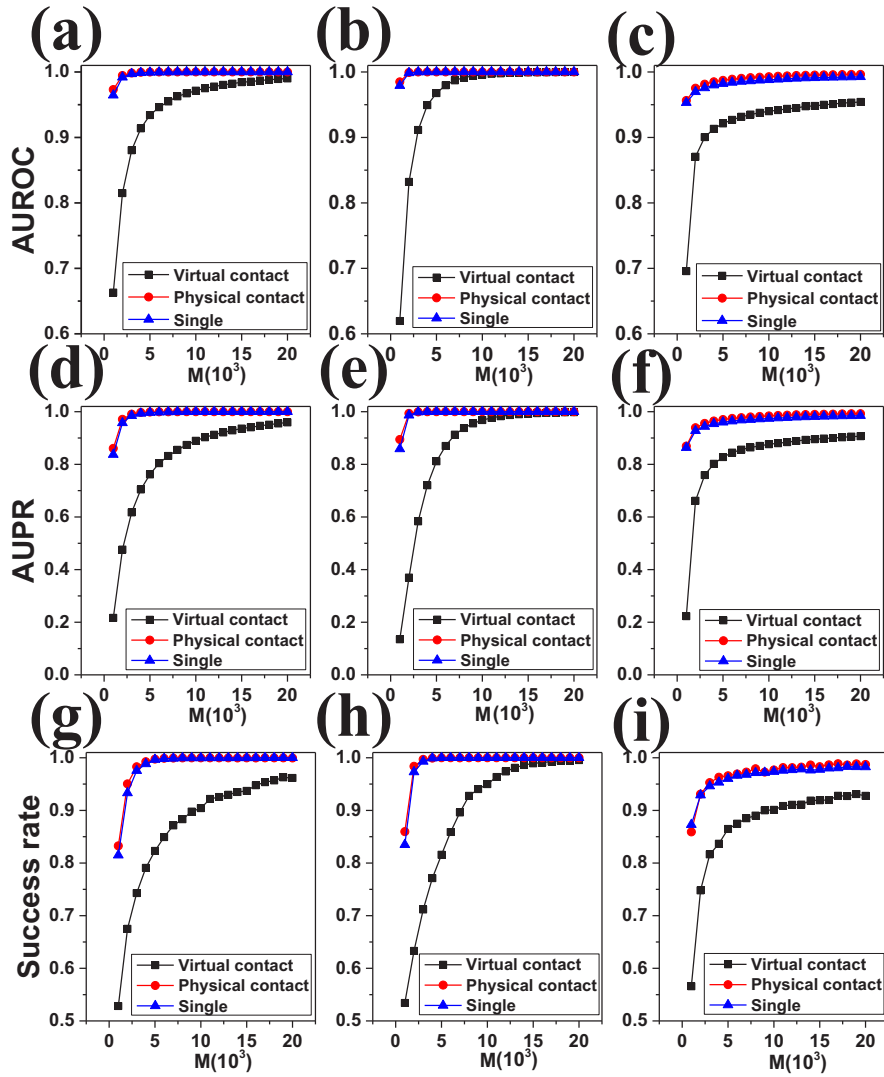


**Figure 4.** Reconstruction accuracy of MITSEN0810 and MITSEN0904 networks. (a)–(c) For the MITSEN0810 network, values of the AUROC, AUPR, and Success rate versus length  $M$  of the time series, respectively, for the parameter setting  $\lambda = 0.05$ ,  $\beta_U = 0.2$ ,  $\beta_A = 0.5\beta_U$ , and  $\mu = \delta = 0.8$ . (d)–(f) The corresponding results for the MITSEN0904 network for the same parameter values as for (a)–(c).

BA-BA duplex network due to the difficulty in reconstructing the neighbors of large degree nodes.

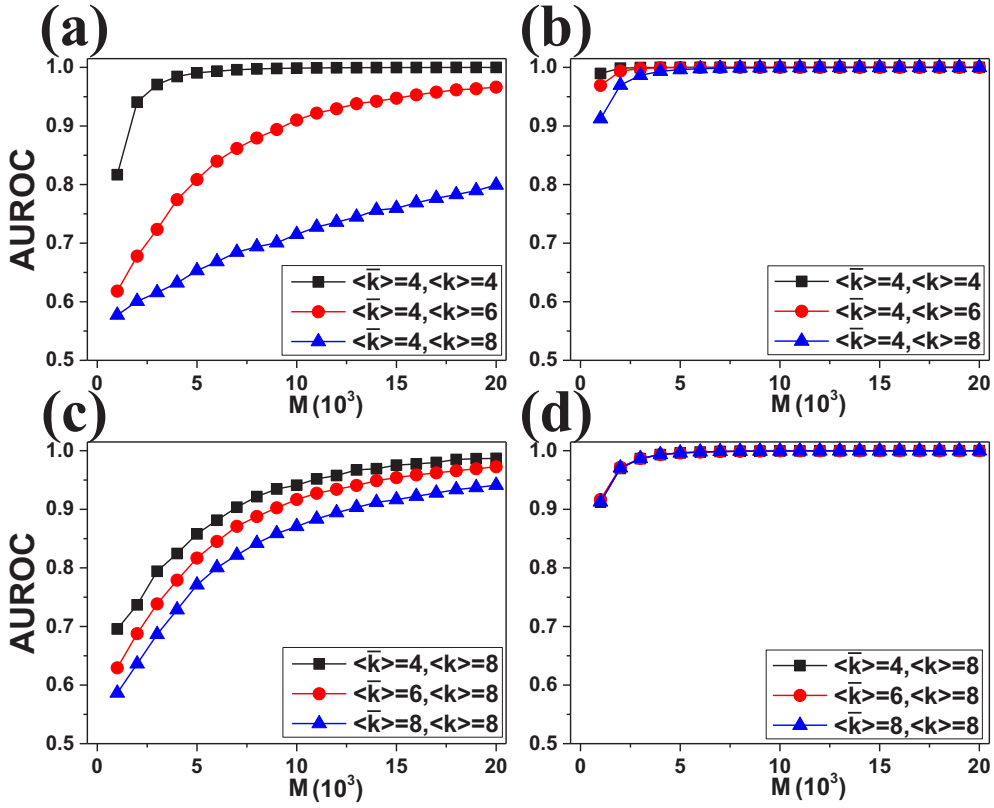
How does the average degree of each layer affect the reconstruction accuracy? Figure 6(a) shows that an increase in the average degree  $\langle k \rangle$  of the physical layer can greatly reduce the reconstruction accuracy of the virtual layer. An explanation is that the probability of being infected tends to increase for a larger value of  $\langle k \rangle$ , “hiding” the information required for uncovering the structure of the virtual layer. Figure 6(b) shows that, for the physical layer, the accuracy gradually decreases with its average degree, for a fixed average degree of the virtual layer. We also find that increasing the average degree  $\langle \bar{k} \rangle$  of the virtual layer tends to reduce the reconstruction accuracy of itself (Figure 6(c)) but has a negligible effect on the reconstruction of the physical layer (Figure 6(d)).

Figure 7 shows the effect of noise on the reconstruction accuracy, where noise is implemented by randomly flipping a fraction  $\tau$  of the states among the total number  $MN$  of states. Noise has a significant effect on the reconstruction of the virtual layer, but it hardly affects the reconstruction of the physical layer (even when the flip rate is  $\tau = 20\%$ ).



**Figure 5.** Effect of interlayer coupling on reconstruction accuracy. Columns 1–3: reconstruction performance for ER-ER, SW-SW, and BA-BA duplex networks, respectively. The “single” case indicates the absence of interlayer coupling:  $\beta_U = 0$  ( $\lambda = 0$ ) for the virtual (physical) layer. The parameter setting is  $\lambda = 0.4$ ,  $\beta_U = 0.4$ ,  $\beta_A = 0.5\beta_U$ , and  $\mu = \delta = 0.8$ . The structures of the two layers are identical. The network parameters are  $N = 100$  and  $\langle k \rangle = \langle k \rangle = 6$ .

**5. Discussion and conclusion.** We have developed a mean-field based MLE framework to solve the challenging problem of data based reconstruction of multiplex networks. The reconstruction performance has been demonstrated using a number of real-world and synthetic duplex networks comprising a virtual and a physical layer, where each layer hosts a distinct type of spreading dynamics that are coupled through the duplex network structure. Extensive tests and analysis indicate that the framework is capable of accurately reconstructing the full topology of each layer based solely on measured time series. A thorough examination of the dynamical coupling between the two layers gives that the reconstruction accuracy of the physical layer is generally much higher than that of the virtual layer. In addition, the



**Figure 6.** Effect of average degree on reconstruction as measured by the AUROC index. (a), (b) For a fixed value of the average degree  $\langle \bar{k} \rangle$  of the virtual layer, the effect of varying the average degree  $\langle k \rangle$  of the physical layer on the reconstruction accuracy of the former and latter, respectively. (c), (d) For a fixed value of  $\langle k \rangle$ , the effect of varying the value of  $\langle \bar{k} \rangle$  on the reconstruction accuracy of the virtual and physical layer, respectively. ER-ER duplex networks with  $N = 100$  are used. The parameters are  $\lambda = 0.3$ ,  $\beta_U = 0.4$ ,  $\beta_A = 0.5\beta_U$ , and  $\mu = \delta = 0.8$ .

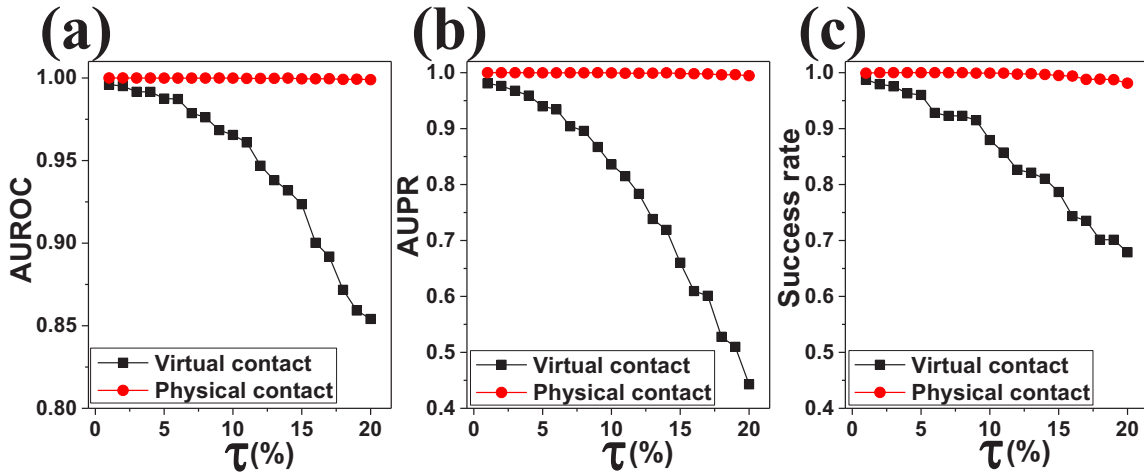


**Figure 7.** Impact of noise on reconstruction accuracy. (a)–(c) AUROC, AUPR, and Success rate versus the fraction  $\tau$  of randomly flipped states for an ER-ER duplex system. The network parameters are  $N = 100$ ,  $\langle \bar{k} \rangle = 4$ , and  $\langle k \rangle = 6$ . The length of the time series is  $M = 30000$ . Other parameters are the same as in Figure 6.

reconstruction accuracy of the virtual layer is more sensitive to external noise than that of the physical layer.

Our framework represents a starting point toward reconstructing more general multiplex networks hosting different types of dynamics. Appealing features are that the framework has high accuracy, is readily implemented, and has a solid mathematical foundation. Issues warranting further considerations include extension to continuous-time dynamical processes, generalization to multiplex networks consisting of more than two layers, and development of effective and practical methods to reduce the required data amount.

**Appendix A. Reconstruction framework of physical layer.** To infer the neighbors of node  $i$  in the physical layer, we need to use some mathematical skills to bypass the two unknown parameters in  $L_2$  (see (3.5)):  $\beta_U^i$  and  $\beta_A^i$ . According to mean-field approximation, one has

$$(A.1) \quad \sum_{j \neq i} s_{t_m}^j b_j^i \approx \frac{k^i}{N-1} \theta_{t_m}^i,$$

where  $k^i$  is the degree of node  $i$  and  $\theta_{t_m}^i = \sum_{j \neq i} s_{t_m}^j$  is the number of I-nodes in the physical layer (excluding node  $i$  itself).

Then, by setting

$$(A.2) \quad \begin{aligned} \gamma_U^i &= (1 - \beta_U^i)^{\frac{k^i}{N-1}}, \\ \gamma_A^i &= (1 - \beta_A^i)^{\frac{k^i}{N-1}}, \end{aligned}$$

we write (3.5) concisely as

$$(A.3) \quad \hat{L}_2(\gamma_U^i, \gamma_A^i) = \sum_m \left\{ \begin{aligned} & \left[ X_{U,t_m}^i \ln \left( (\gamma_U^i)^{\theta_{t_m}^i} \right) + Y_{U,t_m}^i \ln \left( 1 - (\gamma_U^i)^{\theta_{t_m}^i} \right) \right] \\ & + \left[ X_{A,t_m}^i \ln \left( (\gamma_A^i)^{\theta_{t_m}^i} \right) + Y_{A,t_m}^i \ln \left( 1 - (\gamma_A^i)^{\theta_{t_m}^i} \right) \right] \end{aligned} \right\}.$$

Taking the derivatives of  $\hat{L}_2$  with respect to  $\gamma_U^i$  and  $\gamma_A^i$  and setting them to zero, we get

$$(A.4) \quad \begin{aligned} \sum_m Y_{U,t_m}^i \theta_{t_m}^i \frac{(\gamma_U^i)^{\theta_{t_m}^i}}{1 - (\gamma_U^i)^{\theta_{t_m}^i}} &= \sum_m X_{U,t_m}^i \theta_{t_m}^i, \\ \sum_m Y_{A,t_m}^i \theta_{t_m}^i \frac{(\gamma_A^i)^{\theta_{t_m}^i}}{1 - (\gamma_A^i)^{\theta_{t_m}^i}} &= \sum_m X_{A,t_m}^i \theta_{t_m}^i, \end{aligned}$$

which gives the values of  $\gamma_U^i = \tilde{\gamma}_U^i$  and  $\gamma_A^i = \tilde{\gamma}_A^i$ , respectively.

Similar to the mean-field analysis of the virtual layer, we differentiate (3.5) with respect to  $b_l^i$  and set it to zero:

$$(A.5) \quad \begin{aligned} & \sum_m \left\{ \begin{aligned} & \ln \left( 1 - \beta_U^i \right) s_{t_m}^l Y_{U,t_m}^i \frac{(1 - \beta_U^i)^{\sum_{j \neq i} b_j^i s_{t_m}^j}}{1 - (1 - \beta_U^i)^{\sum_{j \neq i} b_j^i s_{t_m}^j}} \\ & + \ln \left( 1 - \beta_A^i \right) s_{t_m}^l Y_{A,t_m}^i \frac{(1 - \beta_A^i)^{\sum_{j \neq i} b_j^i s_{t_m}^j}}{1 - (1 - \beta_A^i)^{\sum_{j \neq i} b_j^i s_{t_m}^j}} \end{aligned} \right\} \\ & = \sum_m \left\{ \ln \left( 1 - \beta_U^i \right) X_{U,t_m}^i s_{t_m}^l + \ln \left( 1 - \beta_A^i \right) X_{A,t_m}^i s_{t_m}^l \right\}. \end{aligned}$$

With the assumption in (A.2) and setting  $\rho = \frac{\ln \tilde{\gamma}_U^i}{\ln \tilde{\gamma}_A^i} = \frac{\ln(1-\beta_U^i)}{\ln(1-\beta_A^i)}$ , we can further simplify (A.5) as

$$(A.6) \quad \begin{aligned} & \sum_m \left[ \rho s_{t_m}^l Y_{U,t_m}^i \frac{(1-\beta_U^i)^{\sum_{j \neq i} b_j^i s_{t_m}^j}}{1-(1-\beta_U^i)^{\sum_{j \neq i} b_j^i s_{t_m}^j}} + s_{t_m}^l Y_{A,t_m}^i \frac{(1-\beta_A^i)^{\sum_{j \neq i} b_j^i s_{t_m}^j}}{1-(1-\beta_A^i)^{\sum_{j \neq i} b_j^i s_{t_m}^j}} \right] \\ & = \sum_m \left[ \rho X_{U,t_m}^i s_{t_m}^l + X_{A,t_m}^i s_{t_m}^l \right]. \end{aligned}$$

Let  $x = \sum_{j \neq i} b_j^i s_{t_m}^j$ ,  $x_0 = \frac{k^i}{N-1} \theta_{t_m}^i$  ( $x \approx x_0$  from the mean-field approximation in (A.1)), and  $a = 1 - \beta_U^i$ . One has  $a^{x_0} = (\tilde{\gamma}_U^i)^{\theta_{t_m}^i}$  from (A.2). Using (3.10), the following equation is obtained:

$$(A.7) \quad \frac{(1-\beta_U^i)^{\sum_{j \neq i} b_j^i s_{t_m}^j}}{1-(1-\beta_U^i)^{\sum_{j \neq i} b_j^i s_{t_m}^j}} = F_{U,t_m}^i + G_{U,t_m}^i \ln(1-\beta_U^i) \sum_{j \neq i} b_j^i s_{t_m}^j,$$

where  $F_{U,t_m}^i = \frac{(\tilde{\gamma}_U^i)^{\theta_{t_m}^i}}{1-(\tilde{\gamma}_U^i)^{\theta_{t_m}^i}} - \frac{(\tilde{\gamma}_U^i)^{\theta_{t_m}^i}}{(1-(\tilde{\gamma}_U^i)^{\theta_{t_m}^i})^2} \theta_{t_m}^i \ln \tilde{\gamma}_U^i$  and  $G_{U,t_m}^i = \frac{(\tilde{\gamma}_U^i)^{\theta_{t_m}^i}}{(1-(\tilde{\gamma}_U^i)^{\theta_{t_m}^i})^2}$ .

Again, setting  $a^{x_0} = (\tilde{\gamma}_A^i)^{\theta_{t_m}^i}$  and using (3.10) leads to

$$(A.8) \quad \frac{(1-\beta_A^i)^{\sum_{j \neq i} b_j^i s_{t_m}^j}}{1-(1-\beta_A^i)^{\sum_{j \neq i} b_j^i s_{t_m}^j}} = F_{A,t_m}^i + G_{A,t_m}^i \ln(1-\beta_A^i) \sum_{j \neq i} b_j^i s_{t_m}^j,$$

where

$$F_{A,t_m}^i = \frac{(\tilde{\gamma}_A^i)^{\theta_{t_m}^i}}{1-(\tilde{\gamma}_A^i)^{\theta_{t_m}^i}} - \frac{(\tilde{\gamma}_A^i)^{\theta_{t_m}^i}}{(1-(\tilde{\gamma}_A^i)^{\theta_{t_m}^i})^2} \theta_{t_m}^i \ln \tilde{\gamma}_A^i \quad \text{and} \quad G_{A,t_m}^i = \frac{(\tilde{\gamma}_A^i)^{\theta_{t_m}^i}}{(1-(\tilde{\gamma}_A^i)^{\theta_{t_m}^i})^2}.$$

With the above approximations, (A.6) can be written in the linear systems of equations:

$$(A.9) \quad \begin{aligned} & \sum_m \left[ \left( \rho^2 Y_{U,t_m}^i G_{U,t_m}^i + Y_{A,t_m}^i G_{A,t_m}^i \right) s_{t_m}^l \ln(1-\beta_A^i) \sum_{j \neq i} b_j^i s_{t_m}^j \right] \\ & = \sum_m \left( \rho X_{U,t_m}^i + X_{A,t_m}^i - \rho Y_{U,t_m}^i F_{U,t_m}^i - Y_{A,t_m}^i F_{A,t_m}^i \right) s_{t_m}^l. \end{aligned}$$

Equation (A.9) can be further rewritten as (3.14) by letting  $\Phi_{t_m}^i = \rho^2 Y_{U,t_m}^i G_{U,t_m}^i + Y_{A,t_m}^i G_{A,t_m}^i$  and  $\Gamma_{t_m}^i = \rho X_{U,t_m}^i + X_{A,t_m}^i - \rho Y_{U,t_m}^i F_{U,t_m}^i - Y_{A,t_m}^i F_{A,t_m}^i$ .

**Appendix B. Selection of threshold value for identification of existent links.** For each node  $i$ , the values of  $a_i^j \ln(1-\lambda^i)$  (or of  $b_i^j \ln(1-\beta_A^i)$ ) can be obtained from (3.12) (or (3.14)).

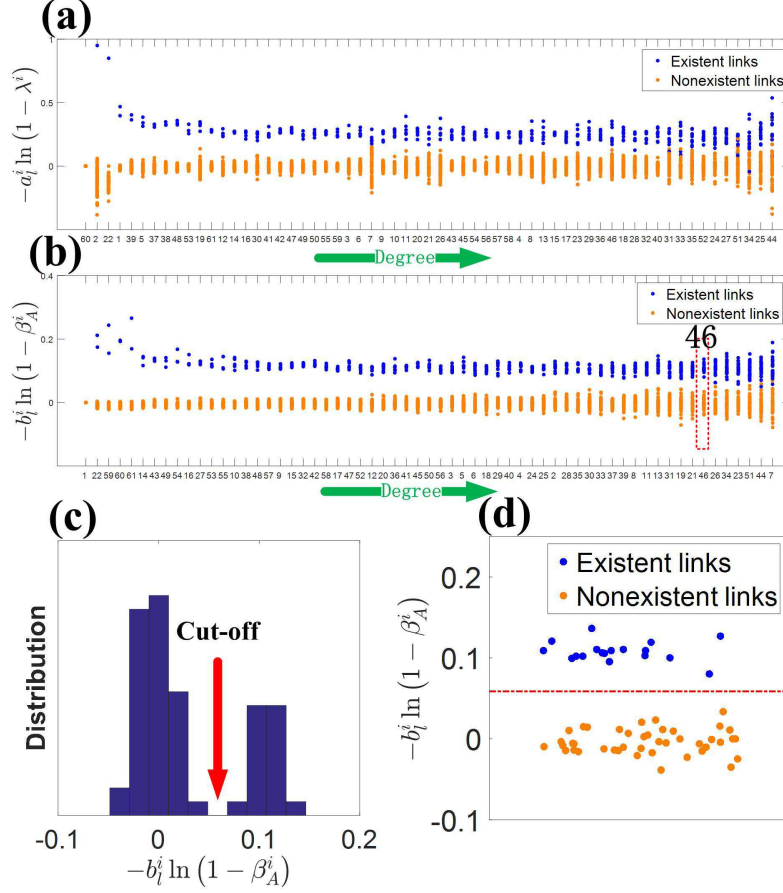


**Figure 8.** Reconstruction of CS-AARHUS duplex network. (a), (b) Values of  $-a_l^i \ln(1 - \lambda^i)$ ,  $i \neq l$ , and  $-b_l^i \ln(1 - \beta_A^i)$ ,  $i \neq l$  for each node, respectively. Each column gives the connectivity of a node. The blue and orange points denote the existent and nonexistent links, respectively. (c) Illustration of the choice of the threshold with node 46 (highlighted by the red dashed frame in (b)). Shown is the distribution of the values of  $-b_l^{46} \ln(1 - \lambda^i)$  for  $l \neq 46$ . The peak centered about zero corresponds to nonexistent links, while the other peak corresponds to existent links. A threshold can be set within the gap between the two peaks. (d) The threshold is illustrated to distinguish the actual from the nonexistent links. The length of time series is  $M = 30000$ . Other parameters are  $\lambda = 0.2$ ,  $\beta_U = 0.2$ ,  $\beta_A = 0.5\beta_U$ , and  $\mu = \delta = 0.8$ .

From Figures 8(a), (b), we have that the values of  $-a_l^i \ln(1 - \lambda^i)$  (or  $-b_l^i \ln(1 - \beta_A^i)$ ) are unequivocally above zero for the existent links, while their values are close to zero for nonexistent links, with a gap between the two sets of values. Representing the values listed in each column as a histogram, we have that the peak centered about zero corresponds to nonexistent links and the other corresponds to existent links. A threshold value can be placed between the two peaks [37], as shown in Figure 8(c). A pair of nodes  $i$  and  $l$  are connected if the corresponding value of  $-a_l^i \ln(1 - \lambda^i)$  [ $-b_l^i \ln(1 - \beta_A^i)$ ] is larger than the threshold. Take node 46 as an example. We wish to infer its neighbors in the physical layer (highlighted by the red dashed

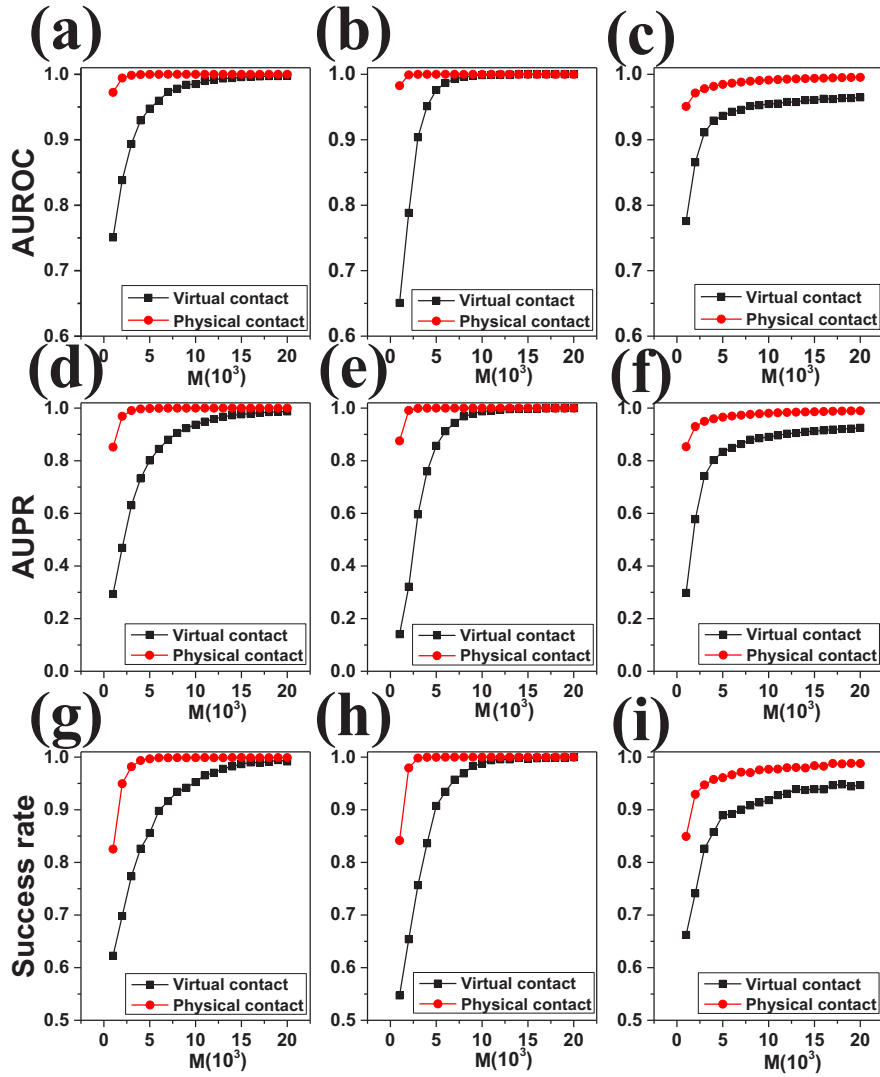


**Figure 9.** Applicability of reconstruction framework to spreading dynamics with heterogeneous rates. Reconstruction accuracy versus the length  $M$  of the time series for ER-ER (left column), SW-SW (central column), and BA-BA (right column) duplex networks with heterogeneous transmission and recovery rates. The network parameters are  $N = 100$  and  $\langle \bar{k} \rangle = 4$ ,  $\langle k \rangle = 6$ .

frame in Figure 8(b)). Figure 8(d) shows that the values larger than the threshold correspond to the existent links.

**Appendix C. Reconstruction of duplex networks with heterogeneous rates of spreading dynamics.** Figure 9 demonstrates that our framework can reconstruct duplex networks with heterogeneous rates of spreading dynamics. In particular, transmission rates  $\lambda^i$  and  $\beta_U^i$  are randomly chosen from the ranges (0.2, 0.4) and (0.3, 0.5), respectively. The recovery rates  $\delta^i$  and  $\mu^i$  are randomly picked up from the ranges (0.6, 1) and (0.6, 1), respectively. Note that  $\beta_A^i = 0.5\beta_U^i$ .

**Appendix D. Evaluation metrics.** We use three metrics [24] to characterize the performance of our reconstruction framework: the area under the receiver operating characteristic curve (AUROC), the area under the precision-recall curve (AUPR), and the Success rate.

To define AUROC and AUPR, it is necessary to calculate three basic quantities: TPR (true positive rate), FPR (false positive rate), and Recall [24]. In particular, TPR is defined as

$$(D.1) \quad \text{TPR}(l) = \frac{\text{TP}(l)}{T},$$

where  $l$  is the cut-off index in the list of the predicted links,  $\text{TP}(l)$  is the number of true positives in the top  $l$  predictions in the link list, and  $T$  is the number of positives.

FPR is defined as

$$(D.2) \quad \text{FPR}(l) = \frac{\text{FP}(l)}{Q},$$

where  $\text{FP}(l)$  is the number of false positives in the top  $l$  entries in the predicted link list, and  $Q$  is the number of negatives by the golden standard.

Recall and Precision are defined as

$$(D.3) \quad \text{Recall}(l) = \text{TPR}(l) = \frac{\text{TP}(l)}{T}$$

and

$$(D.4) \quad \text{Precision}(l) = \frac{\text{TP}(l)}{\text{TP}(l) + \text{FP}(l)} = \frac{\text{TP}(l)}{l},$$

respectively. Varying the value of  $l$  from 0 to  $N$ , we plot two sequences of points:  $[\text{FPR}(l), \text{TPR}(l)]$  and  $[\text{Recall}(l), \text{Precision}(l)]$ . The area under the two curves corresponds to the values of AUROC and AUPR, respectively. For perfect reconstruction, we have  $\text{AUROC}=1$  and  $\text{AUPR}=1$ . In the worst case (completely random), we have  $\text{AUROC}=0.5$  and  $\text{AUPR}=T/2N$ .

Let  $n_1$  and  $n_2$  be the numbers of the existent and non-existent links in the network, respectively, and  $n_3$  and  $n_4$  be the numbers of the predicted existent and non-existent links. The Success rates for existent links (SREL) and non-existent links (SRNL) are defined as  $n_3/n_1$  and  $n_4/n_2$ , respectively. The normalized Success rate is  $\sqrt{\text{SREL} \times \text{SRNL}}$  [37].

## Appendix E. Reconstruction of duplex networks with UAU-SIR dynamics.

**E.1. UAU-SIR dynamics on duplex networks.** Different from the UAU-SIS model, epidemic dynamics in the physical layer are of the SIR type [51]. An infected (I) node can infect its susceptible (S) neighbors with probability  $\beta$  and meanwhile can be recovered with probability  $\mu$ . The recovered (R) nodes cannot be infected again. Henceforth, each node within the UAU-SIR model has five potential states: aware and susceptible (AS), aware and infective (AI), aware and recovered (AR), unaware and susceptible (US), unaware and recovered (UR).

Let  $\bar{s}_t^i$  and  $s_t^i$  denote the state of node  $i$  at time  $t$  in the virtual layer and the physical layer, respectively.  $\bar{s}_t^i = 0$  (or 1) indicates that node  $i$  is in a U-state (A-state), and  $s_t^i = 0$

(1 or 2) indicates that node  $i$  is in an S-state (I-state or R-state). Therefore,  $\sum_{j \neq i} a_j^i I(\bar{s}_t^j, 1)$  (or  $\sum_{j \neq i} b_j^i I(s_t^j, 1)$ ) depicts the number of A-neighbors (I-neighbors) of node  $i$ , where  $I(x, y) = 1$  when  $x = y$ , and otherwise  $I(x, y) = 0$ .

Similar to the UAU-SIS model, the three probabilities describing the UAU-SIR spreading dynamics are given as

$$(E.1) \quad \begin{aligned} r_t^i &= (1 - \lambda^i) \sum_{j \neq i} a_j^i I(\bar{s}_t^j, 1), \\ q_{U,t}^i &= (1 - \beta_U^i) \sum_{j \neq i} b_j^i I(s_t^j, 1), \\ q_{A,t}^i &= (1 - \beta_A^i) \sum_{j \neq i} b_j^i I(s_t^j, 1). \end{aligned}$$

Figure 10 presents the transition probability tree of the UAU-SIR coupling dynamics on the duplex networks.

Figure 10 and (E.1) imply that the transition probabilities of node  $i$  from the US state to the US, AS, and AI states are

$$(E.2) \quad \begin{aligned} P^{US \rightarrow US} &= r_t^i q_{U,t}^i, \\ P^{US \rightarrow AS} &= (1 - r_t^i) q_{U,t}^i, \\ P^{US \rightarrow AI} &= r_t^i (1 - q_{U,t}^i) + (1 - r_t^i) (1 - q_{U,t}^i) = 1 - q_{U,t}^i. \end{aligned}$$

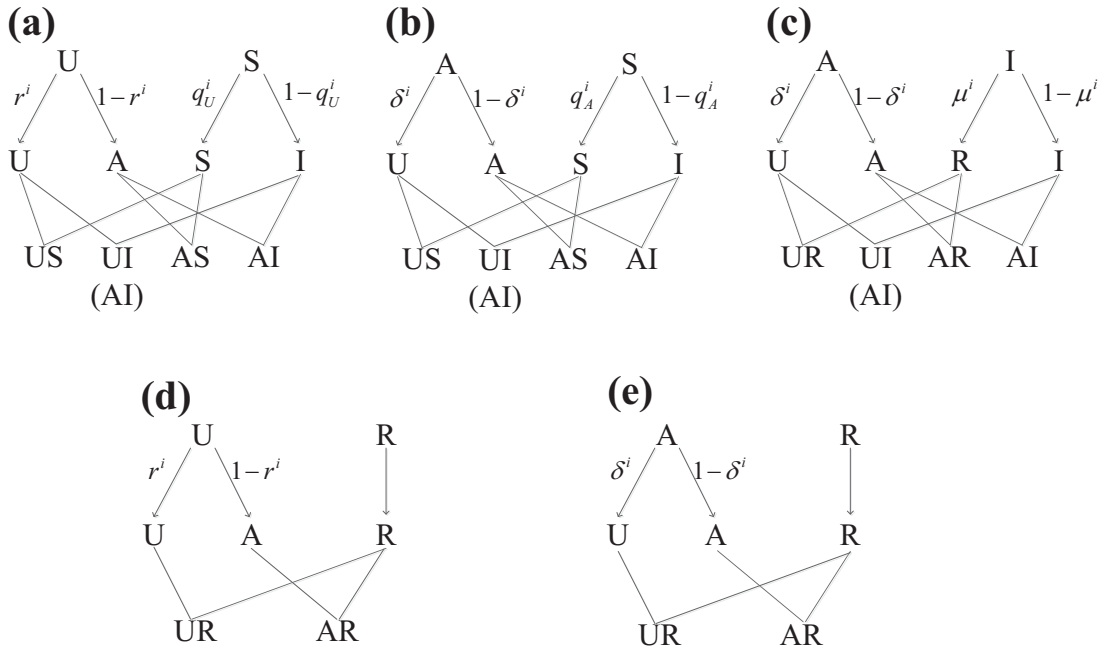


**Figure 10.** Transition probability tree of coupled UAU-SIR dynamics on duplex networks. AI, aware and infected; UI, unaware and infected (redundant to the AI state); AS, aware and susceptible; AR, aware and recovered; US, unaware and susceptible; and UR, unaware and recovered.

The transition probabilities of node  $i$  from the AS state to the US, AS, and AI states are

$$(E.3) \quad \begin{aligned} P^{AS \rightarrow US} &= \delta^i q_{A,t}^i, \\ P^{AS \rightarrow AS} &= (1 - \delta^i) q_{A,t}^i, \\ P^{AS \rightarrow AI} &= \delta^i (1 - q_{A,t}^i) + (1 - \delta^i) (1 - q_{A,t}^i) = 1 - q_{A,t}^i. \end{aligned}$$

The transition probabilities of node  $i$  from the AI state to the UR, AR, and AI states are

$$(E.4) \quad \begin{aligned} P^{AI \rightarrow UR} &= \delta^i \mu^i, \\ P^{AI \rightarrow AR} &= (1 - \delta^i) \mu^i, \\ P^{AI \rightarrow AI} &= 1 - \mu^i. \end{aligned}$$

The transition probabilities of node  $i$  from the UR state to the UR and AR states are

$$(E.5) \quad \begin{aligned} P^{UR \rightarrow UR} &= r_t^i, \\ P^{UR \rightarrow AR} &= 1 - r_t^i. \end{aligned}$$

Also, the transition probabilities of node  $i$  from the AR state to the UR and AR states are

$$(E.6) \quad \begin{aligned} P^{AR \rightarrow UR} &= \delta^i, \\ P^{AR \rightarrow AR} &= 1 - \delta^i. \end{aligned}$$

**E.2. Establish the likelihood function.** For node  $i$ , if we know all nodes' states in two layers, its connections in the virtual and physical layers, and the parameters in the dynamics, then the joint probability (likelihood function) of node  $i$  at the all next time states is

$$(E.7) \quad P \left( \left\{ \bar{s}_{t_m+1}^i, s_{t_m+1}^i \right\}_{m=1 \dots M} \left\{ \bar{s}_{t_m}^j, s_{t_m}^j \right\}_{j=1 \dots N, m=1 \dots M}, \mathbf{a}^i, \mathbf{b}^i, \lambda^i, \beta_U^i, \beta_A^i, \delta^i, \mu^i \right) \\ = \prod_m \left\{ \begin{aligned} & \left[ \begin{aligned} & \left( r_{t_m}^i q_{U,t_m}^i \right)^{I(\bar{s}_{t_m+1}^i, 0) I(s_{t_m+1}^i, 0)} \left( 1 - q_{U,t_m}^i \right)^{I(\bar{s}_{t_m+1}^i, 1) I(s_{t_m+1}^i, 1)} \\ & \times \left( (1 - r_{t_m}^i) q_{U,t_m}^i \right)^{I(\bar{s}_{t_m+1}^i, 1) I(s_{t_m+1}^i, 0)} \end{aligned} \right]^{I(\bar{s}_{t_m}^i, 0) I(s_{t_m}^i, 0)} \\ & \times \left[ \begin{aligned} & \left( \delta^i q_{A,t_m}^i \right)^{I(\bar{s}_{t_m+1}^i, 0) I(s_{t_m+1}^i, 0)} \left( 1 - q_{A,t_m}^i \right)^{I(\bar{s}_{t_m+1}^i, 1) I(s_{t_m+1}^i, 1)} \\ & \times \left( (1 - \delta^i) q_{A,t_m}^i \right)^{I(\bar{s}_{t_m+1}^i, 1) I(s_{t_m+1}^i, 0)} \end{aligned} \right]^{I(\bar{s}_{t_m}^i, 1) I(s_{t_m}^i, 0)} \\ & \times \left[ \begin{aligned} & \left( \delta^i \mu^i \right)^{I(\bar{s}_{t_m+1}^i, 0) I(s_{t_m+1}^i, 2)} \left( 1 - \mu^i \right)^{I(\bar{s}_{t_m+1}^i, 1) I(s_{t_m+1}^i, 1)} \\ & \times \left( (1 - \delta^i) \mu^i \right)^{I(\bar{s}_{t_m+1}^i, 1) I(s_{t_m+1}^i, 2)} \end{aligned} \right]^{I(\bar{s}_{t_m}^i, 1) I(s_{t_m}^i, 1)} \\ & \times \left[ \begin{aligned} & \left( r_{t_m}^i \right)^{I(\bar{s}_{t_m+1}^i, 0) I(s_{t_m+1}^i, 2)} \left( 1 - r_{t_m}^i \right)^{I(\bar{s}_{t_m+1}^i, 1) I(s_{t_m+1}^i, 2)} \\ & \times \left( \delta^i \right)^{I(\bar{s}_{t_m+1}^i, 0) I(s_{t_m+1}^i, 2)} \left( 1 - \delta^i \right)^{I(\bar{s}_{t_m+1}^i, 1) I(s_{t_m+1}^i, 2)} \end{aligned} \right]^{I(\bar{s}_{t_m}^i, 0) I(s_{t_m}^i, 2)} \\ & \times \left[ \begin{aligned} & \left( \delta^i \right)^{I(\bar{s}_{t_m+1}^i, 0) I(s_{t_m+1}^i, 2)} \left( 1 - \delta^i \right)^{I(\bar{s}_{t_m+1}^i, 1) I(s_{t_m+1}^i, 2)} \\ & \times \left( \delta^i \right)^{I(\bar{s}_{t_m+1}^i, 0) I(s_{t_m+1}^i, 2)} \left( 1 - \delta^i \right)^{I(\bar{s}_{t_m+1}^i, 1) I(s_{t_m+1}^i, 2)} \end{aligned} \right]^{I(\bar{s}_{t_m}^i, 1) I(s_{t_m}^i, 2)} \end{aligned} \right\}.$$

The quantity  $L_1(\mathbf{a}^i, \lambda^i)$  that depends on the connectivity of node  $i$  in the virtual layer is given by

$$(E.8) \quad L_1(\mathbf{a}^i, \lambda^i) = \sum_m \left[ \begin{array}{l} \bar{X}_{t_m}^i \ln \left( (1 - \lambda^i)^{\sum_{j \neq i} a_j^i \mathbb{I}(\bar{s}_{t_m}^j, 1)} \right) \\ + \bar{Y}_{t_m}^i \ln \left( 1 - (1 - \lambda^i)^{\sum_{j \neq i} a_j^i \mathbb{I}(\bar{s}_{t_m}^j, 1)} \right) \end{array} \right],$$

where

$$(E.9) \quad \begin{aligned} \bar{X}_{t_m}^i &= \mathbb{I}(\bar{s}_{t_m+1}^i, 0) \mathbb{I}(\bar{s}_{t_m}^i, 0) [\mathbb{I}(s_{t_m+1}^i, 0) \mathbb{I}(s_{t_m}^i, 0) + \mathbb{I}(s_{t_m+1}^i, 2) \mathbb{I}(s_{t_m}^i, 2)], \\ \bar{Y}_{t_m}^i &= \mathbb{I}(\bar{s}_{t_m+1}^i, 1) \mathbb{I}(\bar{s}_{t_m}^i, 0) [\mathbb{I}(s_{t_m+1}^i, 0) \mathbb{I}(s_{t_m}^i, 0) + \mathbb{I}(s_{t_m+1}^i, 2) \mathbb{I}(s_{t_m}^i, 2)]. \end{aligned}$$

Similarly, the quantity  $L_2(\mathbf{b}^i, \beta_U^i, \beta_A^i)$  that depends on the connectivity of node  $i$  in the physical layer is given by

$$(E.10) \quad L_2(\mathbf{b}^i, \beta_U^i, \beta_A^i) = \sum_m \left\{ \begin{array}{l} \left[ \begin{array}{l} X_{U,t_m}^i \ln \left( (1 - \beta_U^i)^{\sum_{j \neq i} b_j^i \mathbb{I}(s_{t_m}^j, 1)} \right) \\ + Y_{U,t_m}^i \ln \left( 1 - (1 - \beta_U^i)^{\sum_{j \neq i} b_j^i \mathbb{I}(s_{t_m}^j, 1)} \right) \end{array} \right] \\ + \left[ \begin{array}{l} X_{A,t_m}^i \ln \left( (1 - \beta_A^i)^{\sum_{j \neq i} b_j^i \mathbb{I}(s_{t_m}^j, 1)} \right) \\ + Y_{A,t_m}^i \ln \left( 1 - (1 - \beta_A^i)^{\sum_{j \neq i} b_j^i \mathbb{I}(s_{t_m}^j, 1)} \right) \end{array} \right] \end{array} \right\},$$

where

$$(E.11) \quad \begin{aligned} X_{U,t_m}^i &= \mathbb{I}(\bar{s}_{t_m}^i, 0) \mathbb{I}(s_{t_m}^i, 0) \mathbb{I}(s_{t_m+1}^i, 0), \\ Y_{U,t_m}^i &= \mathbb{I}(\bar{s}_{t_m}^i, 0) \mathbb{I}(s_{t_m}^i, 0) \mathbb{I}(\bar{s}_{t_m+1}^i, 1) \mathbb{I}(s_{t_m+1}^i, 1), \\ X_{A,t_m}^i &= \mathbb{I}(\bar{s}_{t_m}^i, 1) \mathbb{I}(s_{t_m}^i, 0) \mathbb{I}(s_{t_m+1}^i, 0), \\ Y_{A,t_m}^i &= \mathbb{I}(\bar{s}_{t_m}^i, 1) \mathbb{I}(s_{t_m}^i, 0) \mathbb{I}(\bar{s}_{t_m+1}^i, 1) \mathbb{I}(s_{t_m+1}^i, 1). \end{aligned}$$

**E.3. Reconstruction framework of virtual layer.** To infer the neighbors of node  $i$  in the virtual layer, we need to use some mathematical skills to bypass the unknown parameter in  $L_1$  (see (E.8)):  $\lambda^i$ . According to mean-field approximation, one has

$$(E.12) \quad \sum_{j \neq i} \mathbb{I}(\bar{s}_{t_m}^j, 1) a_j^i \approx \frac{\bar{k}^i}{N-1} \bar{\theta}_{t_m}^i,$$

where  $\bar{k}^i$  is the degree of node  $i$  and  $\bar{\theta}_{t_m}^i = \sum_{j \neq i} \mathbb{I}(\bar{s}_{t_m}^j, 1)$  is the number of A-nodes in the virtual layer (excluding node  $i$  itself).

Then, by setting

$$(E.13) \quad \bar{\gamma}^i = (1 - \lambda^i)^{\frac{\bar{k}^i}{N-1}},$$

and similar to (3.7) and (3.8), we get

$$(E.14) \quad \sum_m \bar{Y}_{t_m}^i \bar{\theta}_{t_m}^i \frac{(\bar{\gamma}^i)^{\bar{\theta}_{t_m}^i}}{1 - (\bar{\gamma}^i)^{\bar{\theta}_{t_m}^i}} = \sum_m \bar{X}_{t_m}^i \bar{\theta}_{t_m}^i.$$

From (E.14), one can numerically obtain the solution of  $\bar{\gamma}^i$  (denoted as  $\tilde{\gamma}^i$ ).

Similarly, the connectivity of node  $i$  in the virtual layer (i.e.,  $\mathbf{a}^i$ ) can be inferred by solving the following linear systems of equations:

$$(E.15) \quad \begin{bmatrix} \sum_m \bar{\Phi}_{t_m}^i \bar{I}_{1,1} & \cdots & \sum_m \bar{\Phi}_{t_m}^i \bar{I}_{1,i-1} & \sum_m \bar{\Phi}_{t_m}^i \bar{I}_{1,i+1} & \cdots & \sum_m \bar{\Phi}_{t_m}^i \bar{I}_{1,N} \\ \vdots & & \vdots & \vdots & & \vdots \\ \sum_m \bar{\Phi}_{t_m}^i \bar{I}_{i-1,1} & \cdots & \sum_m \bar{\Phi}_{t_m}^i \bar{I}_{i-1,i-1} & \sum_m \bar{\Phi}_{t_m}^i \bar{I}_{i-1,i+1} & \cdots & \sum_m \bar{\Phi}_{t_m}^i \bar{I}_{i-1,N} \\ \sum_m \bar{\Phi}_{t_m}^i \bar{I}_{i+1,1} & \cdots & \sum_m \bar{\Phi}_{t_m}^i \bar{I}_{i+1,i-1} & \sum_m \bar{\Phi}_{t_m}^i \bar{I}_{i+1,i+1} & \cdots & \sum_m \bar{\Phi}_{t_m}^i \bar{I}_{i+1,N} \\ \vdots & & \vdots & \vdots & & \vdots \\ \sum_m \bar{\Phi}_{t_m}^i \bar{I}_{N,1} & \cdots & \sum_m \bar{\Phi}_{t_m}^i \bar{I}_{N,i-1} & \sum_m \bar{\Phi}_{t_m}^i \bar{I}_{N,i+1} & \cdots & \sum_m \bar{\Phi}_{t_m}^i \bar{I}_{N,N} \end{bmatrix} \times \begin{bmatrix} a_1^i \ln(1 - \lambda^i) \\ \vdots \\ a_{i-1}^i \ln(1 - \lambda^i) \\ a_{i+1}^i \ln(1 - \lambda^i) \\ \vdots \\ a_N^i \ln(1 - \lambda^i) \end{bmatrix} = \begin{bmatrix} \sum_m \bar{\Gamma}_{t_m}^i \mathbf{I}(\bar{s}_{t_m}^1, 1) \\ \vdots \\ \sum_m \bar{\Gamma}_{t_m}^i \mathbf{I}(\bar{s}_{t_m}^{i-1}, 1) \\ \sum_m \bar{\Gamma}_{t_m}^i \mathbf{I}(\bar{s}_{t_m}^{i+1}, 1) \\ \vdots \\ \sum_m \bar{\Gamma}_{t_m}^i \mathbf{I}(\bar{s}_{t_m}^N, 1) \end{bmatrix},$$

where  $\bar{I}_{l,k} = \mathbf{I}(\bar{s}_{t_m}^l, 1)\mathbf{I}(\bar{s}_{t_m}^k, 1)$ ,  $\bar{\Phi}_{t_m}^i = \bar{Y}_{t_m}^i \bar{G}_{t_m}^i$ ,  $\bar{\Gamma}_{t_m}^i = \bar{X}_{t_m}^i - \bar{Y}_{t_m}^i \bar{F}_{t_m}^i$ ,

$$\bar{F}_{t_m}^i = \frac{(\tilde{\gamma}^i)^{\bar{\theta}_{t_m}^i}}{1 - (\tilde{\gamma}^i)^{\bar{\theta}_{t_m}^i}} - \frac{(\tilde{\gamma}^i)^{\bar{\theta}_{t_m}^i}}{(1 - (\tilde{\gamma}^i)^{\bar{\theta}_{t_m}^i})^2} \bar{\theta}_{t_m}^i \ln \tilde{\gamma}^i \quad \text{and} \quad \bar{G}_{t_m}^i = \frac{(\tilde{\gamma}^i)^{\bar{\theta}_{t_m}^i}}{(1 - (\tilde{\gamma}^i)^{\bar{\theta}_{t_m}^i})^2}.$$

**E.4. Reconstruction framework of physical layer.** To infer the neighbors of node  $i$  in the physical layer, we need to use some mathematical skills to bypass the two unknown parameters in  $L_2$  (see (E.10)):  $\beta_U^i$  and  $\beta_A^i$ . According to mean-field approximation, one has

$$(E.16) \quad \sum_{j \neq i} \mathbf{I}(s_{t_m}^j, 1) b_j^i \approx \frac{k^i}{N-1} \theta_{t_m}^i,$$

where  $k^i$  is the degree of node  $i$  and  $\theta_{t_m}^i = \sum_{j \neq i} \mathbf{I}(s_{t_m}^j, 1)$  is the number of I-nodes in the physical layer (excluding node  $i$  itself). Then, by setting

$$(E.17) \quad \begin{aligned} \gamma_U^i &= (1 - \beta_U^i)^{\frac{k^i}{N-1}}, \\ \gamma_A^i &= (1 - \beta_A^i)^{\frac{k^i}{N-1}}, \end{aligned}$$

and similar to (A.3) and (A.4), one has

$$(E.18) \quad \begin{aligned} \sum_m Y_{U,t_m}^i \theta_{t_m}^i \frac{(\gamma_U^i)^{\theta_{t_m}^i}}{1 - (\gamma_U^i)^{\theta_{t_m}^i}} &= \sum_m X_{U,t_m}^i \theta_{t_m}^i, \\ \sum_m Y_{A,t_m}^i \theta_{t_m}^i \frac{(\gamma_A^i)^{\theta_{t_m}^i}}{1 - (\gamma_A^i)^{\theta_{t_m}^i}} &= \sum_m X_{A,t_m}^i \theta_{t_m}^i, \end{aligned}$$

which gives the values of  $\gamma_U^i = \tilde{\gamma}_U^i$  and  $\gamma_A^i = \tilde{\gamma}_A^i$ , respectively.

Similarly, the connectivity of node  $i$  in the physical layer (i.e.,  $\mathbf{b}^i$ ) can be inferred by solving the following linear systems of equations:

$$(E.19) \quad \begin{aligned} &\begin{bmatrix} \sum_m \Phi_{t_m}^i I_{1,1} & \cdots & \sum_m \Phi_{t_m}^i I_{1,i-1} & \sum_m \Phi_{t_m}^i I_{1,i+1} & \cdots & \sum_m \Phi_{t_m}^i I_{1,N} \\ \vdots & & \vdots & \vdots & & \vdots \\ \sum_m \Phi_{t_m}^i I_{i-1,1} & \cdots & \sum_m \Phi_{t_m}^i I_{i-1,i-1} & \sum_m \Phi_{t_m}^i I_{i-1,i+1} & \cdots & \sum_m \Phi_{t_m}^i I_{i-1,N} \\ \sum_m \Phi_{t_m}^i I_{i+1,1} & \cdots & \sum_m \Phi_{t_m}^i I_{i+1,i-1} & \sum_m \Phi_{t_m}^i I_{i+1,i+1} & \cdots & \sum_m \Phi_{t_m}^i I_{i+1,N} \\ \vdots & & \vdots & \vdots & & \vdots \\ \sum_m \Phi_{t_m}^i I_{N,1} & \cdots & \sum_m \Phi_{t_m}^i I_{N,i-1} & \sum_m \Phi_{t_m}^i I_{N,i+1} & \cdots & \sum_m \Phi_{t_m}^i I_{N,N} \end{bmatrix} \\ &\times \begin{bmatrix} b_1^i \ln(1 - \beta_A^i) \\ \vdots \\ b_{i-1}^i \ln(1 - \beta_A^i) \\ b_{i+1}^i \ln(1 - \beta_A^i) \\ \vdots \\ b_N^i \ln(1 - \beta_A^i) \end{bmatrix} = \begin{bmatrix} \sum_m \Gamma_{t_m}^i I(s_{t_m}^1, 1) \\ \vdots \\ \sum_m \Gamma_{t_m}^i I(s_{t_m}^{i-1}, 1) \\ \sum_m \Gamma_{t_m}^i I(s_{t_m}^{i+1}, 1) \\ \vdots \\ \sum_m \Gamma_{t_m}^i I(s_{t_m}^N, 1) \end{bmatrix}, \end{aligned}$$

where  $I_{l,k} = I(s_{t_m}^l, 1)I(s_{t_m}^k, 1)$ ,  $\Phi_{t_m}^i = \rho^2 Y_{U,t_m}^i G_{U,t_m}^i + Y_{A,t_m}^i G_{A,t_m}^i$ ,  $\Gamma_{t_m}^i = \rho X_{U,t_m}^i + X_{A,t_m}^i - \rho Y_{U,t_m}^i F_{U,t_m}^i - Y_{A,t_m}^i F_{A,t_m}^i$ ,  $\rho = \frac{\ln \tilde{\gamma}_U^i}{\ln \tilde{\gamma}_A^i} = \frac{\ln(1 - \beta_U^i)}{\ln(1 - \beta_A^i)}$ ,

$$\begin{aligned} F_{U,t_m}^i &= \frac{(\tilde{\gamma}_U^i)^{\theta_{t_m}^i}}{1 - (\tilde{\gamma}_U^i)^{\theta_{t_m}^i}} - \frac{(\tilde{\gamma}_U^i)^{\theta_{t_m}^i}}{(1 - (\tilde{\gamma}_U^i)^{\theta_{t_m}^i})^2} \theta_{t_m}^i \ln \tilde{\gamma}_U^i, & G_{U,t_m}^i &= \frac{(\tilde{\gamma}_U^i)^{\theta_{t_m}^i}}{(1 - (\tilde{\gamma}_U^i)^{\theta_{t_m}^i})^2}, \\ F_{A,t_m}^i &= \frac{(\tilde{\gamma}_A^i)^{\theta_{t_m}^i}}{1 - (\tilde{\gamma}_A^i)^{\theta_{t_m}^i}} - \frac{(\tilde{\gamma}_A^i)^{\theta_{t_m}^i}}{(1 - (\tilde{\gamma}_A^i)^{\theta_{t_m}^i})^2} \theta_{t_m}^i \ln \tilde{\gamma}_A^i, & \text{and } G_{A,t_m}^i &= \frac{(\tilde{\gamma}_A^i)^{\theta_{t_m}^i}}{(1 - (\tilde{\gamma}_A^i)^{\theta_{t_m}^i})^2}. \end{aligned}$$

**E.5. Reconstructing synthetic duplex networks.** Figure 11 indicates that our framework can reconstruct duplex networks with UAU-SIR spreading dynamics too. Because the SIR epidemic model can cause the nodal states to converge into a stable state, we randomly initialize the states of all nodes whenever there are no I-nodes in the physical layer.

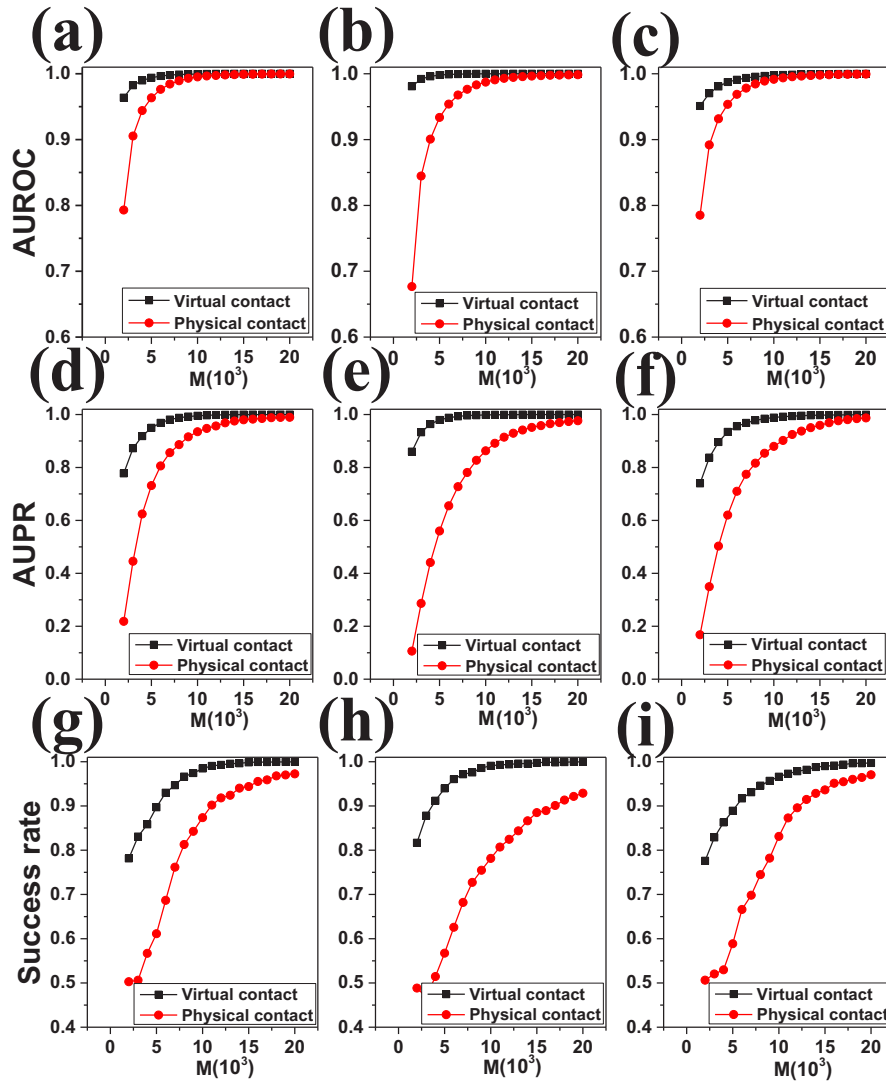


**Figure 11.** Reconstruction accuracy of synthetic duplex networks with UAU-SIR spreading dynamics. Columns 1–3: reconstruction performance for ER-ER, SW-SW, and BA-BA duplex networks, respectively. The parameter setting is  $\lambda = 0.3$ ,  $\beta_U = 0.4$ ,  $\beta_A = 0.5\beta_U$ ,  $\delta = 0.8$ , and  $\mu = 0.6$ . The structures of the two layers are identical. The network parameters are  $N = 100$  and  $\langle \bar{k} \rangle = \langle k \rangle = 6$ .

## REFERENCES

- [1] A.-L. BARABÁSI AND R. ALBERT, *Emergence of scaling in random networks*, Science, 286 (1999), pp. 509–512.
- [2] T. BERRY, F. HAMILTON, N. PEIXOTO, AND T. SAUER, *Detecting connectivity changes in neuronal networks*, J. Neurosci. Methods, 209 (2012), pp. 388–397.
- [3] J. BONGARD AND H. LIPSON, *Automated reverse engineering of nonlinear dynamical systems*, Proc. Natl. Acad. Sci. USA, 104 (2007), pp. 9943–9948.
- [4] A. BROVELLI, M. DING, A. LEDBERG, Y. CHEN, R. NAKAMURA, AND S. L. BRESSLER, *Beta oscillations in a large-scale sensorimotor cortical network: Directional influences revealed by Granger causality*, Proc. Nat. Acad. Sci. USA, 101 (2004), pp. 9849–9854.

- [5] S. V. BULDYREV, R. PARSHANI, G. PAUL, H. E. STANLEY, AND S. HAVLIN, *Catastrophic cascade of failures in interdependent networks*, *Nature*, 464 (2010), pp. 1025–1028.
- [6] J. CASADIEGO, M. NITZAN, S. HALLERBERG, AND M. TIMME, *Model-free inference of direct network interactions from nonlinear collective dynamics*, *Nat. Commun.*, 8 (2017), 2192.
- [7] Y.-Z. CHEN AND Y.-C. LAI, *Sparse dynamical Boltzmann machine for reconstructing complex networks with binary dynamics*, *Phys. Rev. E*, 97 (2018), 032317, <https://doi.org/10.1103/PhysRevE.97.032317>.
- [8] E. S. C. CHING, P.-Y. LAI, AND C. Y. LEUNG, *Extracting connectivity from dynamics of networks with uniform bidirectional coupling*, *Phys. Rev. E*, 88 (2013), 042817, <https://doi.org/10.1103/PhysRevE.88.042817>.
- [9] E. S. C. CHING, P.-Y. LAI, AND C. Y. LEUNG, *Reconstructing weighted networks from dynamics*, *Phys. Rev. E*, 91 (2015), 030801, <https://doi.org/10.1103/PhysRevE.91.030801>.
- [10] M. DE DOMENICO, C. GRANELL, M. A. PORTER, AND A. ARENAS, *The physics of spreading processes in multilayer networks*, *Nat. Phys.*, 12 (2016), pp. 901–906.
- [11] M. DE DOMENICO, A. SOLÉ-RIBALTA, E. COZZO, M. KIVELÄ, Y. MORENO, M. A. PORTER, S. GÓMEZ, AND A. ARENAS, *Mathematical formulation of multilayer networks*, *Phys. Rev. X*, 3 (2013), 041022.
- [12] J. DONGES, Y. ZOU, N. MARWAN, AND J. KURTHS, *The backbone of the climate network*, *Europhys. Lett.*, 87 (2009), 48007.
- [13] V. M. EGUILUZ, D. R. CHIALVO, G. A. CECCHI, M. BALIKI, AND A. V. APKARIAN, *Scale-free brain functional networks*, *Phys. Rev. Lett.*, 94 (2005), 018102.
- [14] P. ERDOS AND A. RÉNYI, *On the evolution of random graphs*, *Publ. Math. Inst. Hung. Acad. Sci.*, 5 (1960), pp. 17–60.
- [15] K. J. FRISTON, *Bayesian estimation of dynamical systems: an application to fMRI*, *NeuroImage*, 16 (2002), pp. 513–530.
- [16] J. GAO, S. V. BULDYREV, H. E. STANLEY, AND S. HAVLIN, *Networks formed from interdependent networks*, *Nat. Phys.*, 8 (2012), pp. 40–48.
- [17] T. S. GARDNER, D. DI BERNARDO, D. LORENZ, AND J. J. COLLINS, *Inferring genetic networks and identifying compound mode of action via expression profiling*, *Science*, 301 (2003), pp. 102–105.
- [18] C. GRANELL, S. GÓMEZ, AND A. ARENAS, *Dynamical interplay between awareness and epidemic spreading in multiplex networks*, *Phys. Rev. Lett.*, 111 (2013), 128701.
- [19] F. HAMILTON, T. BERRY, N. PEIXOTO, AND T. SAUER, *Real-time tracking of neuronal network structure using data assimilation*, *Phys. Rev. E*, 88 (2013), 052715.
- [20] S. HEMPEL, A. KOSESKA, J. KURTHS, AND Z. NIKOLOSKI, *Inner composition alignment for inferring directed networks from short time series*, *Phys. Rev. Lett.*, 107 (2011), 054101.
- [21] J.-Q. KAN AND H.-F. ZHANG, *Effects of awareness diffusion and self-initiated awareness behavior on epidemic spreading—an approach based on multiplex networks*, *Commun. Nonlinear Sci. Numer. Simul.*, 44 (2017), pp. 193–203.
- [22] M. KIVELÄ, A. ARENAS, M. BARTHELEMY, J. P. GLEESON, Y. MORENO, AND M. A. PORTER, *Multilayer networks*, *J. Complex Netw.*, 2 (2014), pp. 203–271.
- [23] Z. LEVNAJĆ AND A. PIKOVSKY, *Network reconstruction from random phase resetting*, *Phys. Rev. Lett.*, 107 (2011), 034101.
- [24] J.-W. LI, Z.-S. SHEN, W.-X. WANG, C. GREBOGI, AND Y.-C. LAI, *Universal data-based method for reconstructing complex networks with binary-state dynamics*, *Phys. Rev. E*, 95 (2017), 032303, <https://doi.org/10.1103/PhysRevE.95.032303>.
- [25] X. LI AND X. LI, *Reconstruction of stochastic temporal networks through diffusive arrival times*, *Nat. Commun.*, 8 (2017), 15729.
- [26] J. LIU, G. MEI, X. WU, AND J. LÜ, *Robust reconstruction of continuously time-varying topologies of weighted networks*, *IEEE Trans. Circuits Systems*, 65 (2018), pp. 2970–2982.
- [27] C. MA, H.-F. ZHANG, AND Y.-C. LAI, *Reconstructing complex networks without time series*, *Phys. Rev. E*, 96 (2017), 022320, <https://doi.org/10.1103/PhysRevE.96.022320>.
- [28] A. MADAN, M. CEBRIAN, S. MOTURU, K. FARRAHI, AND A. S. PENTLAND, *Sensing the “health state” of a community*, *IEEE Pervasive Comput.*, 11 (2012), pp. 36–45, <https://doi.org/10.1109/MPRV.2011.79>.
- [29] M. MAGNANI, B. MICENKOVA, AND L. ROSSI, *Combinatorial Analysis of Multiple Networks*, preprint, [arXiv:1303.4986](https://arxiv.org/abs/1303.4986), 2013.
- [30] G. MEI, X. WU, Y. WANG, M. HU, J.-A. LU, AND G. CHEN, *Compressive-sensing-based structure identification for multilayer networks*, *IEEE Trans. Cybernet*, 48 (2018), pp. 754–764.

- [31] D. NAPOLETANI AND T. D. SAUER, *Reconstructing the topology of sparsely connected dynamical networks*, Phys. Rev. E, 77 (2008), 026103.
- [32] M. NITZAN, J. CASADIEGO, AND M. TIMME, *Revealing physical interaction networks from statistics of collective dynamics*, Sci. Adv., 3 (2017).
- [33] S. PAJEVIC AND D. PLENZ, *Efficient network reconstruction from dynamical cascades identifies small-world topology of neuronal avalanches*, PLoS Comp. Biol., 5 (2009), e1000271.
- [34] G. PIPA AND S. GRÜN, *Non-parametric significance estimation of joint-spike events by shuffling and resampling*, Neurocomp., 52 (2003), pp. 31–37.
- [35] J. REN, W.-X. WANG, B. LI, AND Y.-C. LAI, *Noise bridges dynamical correlation and topology in coupled oscillator networks*, Phys. Rev. Lett., 104 (2010), 058701.
- [36] S. G. SHANDILYA AND M. TIMME, *Inferring network topology from complex dynamics*, New J. Phys., 13 (2011), 013004.
- [37] Z.-S. SHEN, W.-X. WANG, Y. FAN, Z. DI, AND Y.-C. LAI, *Reconstructing propagation networks with natural diversity and identifying hidden sources*, Nat. Commun., 5 (2014), 4323.
- [38] O. STETTER, D. BATTAGLIA, J. SORIANO, AND T. GEISEL, *Model-free reconstruction of excitatory neuronal connectivity from calcium imaging signals*, PLoS Comp. Biol., 8 (2012), e1002653.
- [39] R.-Q. SU, Y.-C. LAI, AND X. WANG, *Identifying chaotic FitzHugh-Nagumo neurons using compressive sensing*, Entropy, 16 (2014), pp. 3889–3902.
- [40] R.-Q. SU, W.-X. WANG, AND Y.-C. LAI, *Detecting hidden nodes in complex networks from time series*, Phys. Rev. E, 85 (2012), 065201.
- [41] J. SUN, D. TAYLOR, AND E. BOLLT, *Causal network inference by optimal causation entropy*, SIAM J. Appl. Dyn. Syst., 14 (2015), pp. 73–106.
- [42] M. TIMME, *Revealing network connectivity from response dynamics*, Phys. Rev. Lett., 98 (2007), 224101.
- [43] M. TIMME AND J. CASADIEGO, *Revealing networks from dynamics: an introduction*, J. Phys. A, 47 (2014), 343001.
- [44] W.-X. WANG, Y.-C. LAI, AND C. GREBOGI, *Data based identification and prediction of nonlinear and complex dynamical systems*, Phys. Rep., 644 (2016), pp. 1–76.
- [45] W.-X. WANG, Y.-C. LAI, C. GREBOGI, AND J.-P. YE, *Network reconstruction based on evolutionary-game data via compressive sensing*, Phys. Rev. X, 1 (2011), 021021.
- [46] W.-X. WANG, R. YANG, Y.-C. LAI, V. KOVANIS, AND M. A. F. HARRISON, *Time-series-based prediction of complex oscillator networks via compressive sensing*, Europhys. Lett., 94 (2011), 48006.
- [47] D. J. WATTS AND S. H. STROGATZ, *Collective dynamics of “small-world” networks*, Nature, 393 (1998), pp. 440–442.
- [48] X. WEI, X. WU, S. CHEN, J. LU, AND G. CHEN, *Cooperative epidemic spreading on a two-layered interconnected network*, SIAM J. Appl. Dyn. Syst., 17 (2018), pp. 1503–1520.
- [49] D. YU, M. RIGHERO, AND L. KOCAREV, *Estimating topology of networks*, Phys. Rev. Lett., 97 (2006), 188701.
- [50] H.-F. ZHANG, F. XU, Z.-K. BAO, AND C. MA, *Reconstructing of networks with binary-state dynamics via generalized statistical inference*, IEEE. Trans. Circuits Systems, 66 (2019), pp. 1608–1619, <https://doi.org/10.1109/TCSI.2018.2886770>.
- [51] C. ZHENG, C. XIA, Q. GUO, AND M. DEHMER, *Interplay between SIR-based disease spreading and awareness diffusion on multiplex networks*, J. Parallel Distr. Com., 115 (2018), pp. 20–28, <https://doi.org/10.1016/j.jpdc.2018.01.001>.
- [52] D. ZHOU, Y. XIAO, Y. ZHANG, Z. XU, AND D. CAI, *Causal and structural connectivity of pulse-coupled nonlinear networks*, Phys. Rev. Lett., 111 (2013), 054102.